J. Fluid Mech. (2008), *vol.* 595, *pp.* 379–408.
doi:10.1017/S002211200700938X Printed in the United Kingdom

Instability of a stratified boundary layer and its coupling with internal gravity waves. Part 1. Linear and nonlinear instabilities

XUESONG WU[1,2] AND JING ZHANG[2]

[1]Department of Mathematics, Imperial College London London SW7 2AZ, UK
[2]Department of Mechanics, Tianjin University, China

(Received 11 April 2006 and in revised form 27 September 2007)

In this paper, we consider a viscous instability of a stratified boundary layer that is a form of the familiar Tollmien–Schlichting (T-S) waves modified by a stable density stratification. As with the usual T-S waves, the triple-deck formalism was employed to provide a self-consistent description of linear and nonlinear instability properties at asymptotically large Reynolds numbers. The effect of stratification on the temporal and spatial linear growth rates is studied. It is found that stratification reduces the maximum spatial growth rate, but enhances the maximum temporal growth rate. This viscous instability may offer a possible alternative explanation for the origin of certain long atmospheric waves, whose characteristics are not well predicted by inviscid instabilities. In the high-frequency limit, the nonlinear evolution of the disturbances is shown to be governed by a nonlinear amplitude equation, which is an extension of the well-known Benjamin–Davis–Ono equation. Numerical solutions indicate that as a spatially isolated disturbance evolves, it radiates a beam of long gravity waves, and meanwhile small-scale ripples develop on its front to form a well-defined wavepacket. It is also shown that for jet-like velocity profiles, the standard triple-deck theory must be adjusted to account for both the displacement and transverse pressure variation induced by the inviscid flow in the main layer. The nonlinear evolution of high-frequency disturbances is governed by a mixed KdV–Benjamin–Davis–Ono equation.

1. Introduction

A stably stratified shear flow over topography can support a variety of waves. The simplest are internal gravity waves (Lighthill 1978). They are sustained simply by the dynamic balance between buoyancy and inertia, and hence can appear in an otherwise static fluid. Internal gravity waves are dynamically stable, and they arise owing to external excitations, such as orographic effects, meteorological fronts and thunderstorms. Specifically, orography forcing on a stratified oncoming flow generates mountain lee waves.

While a density decreasing with height tends to stabilize disturbances, background shear presents a destabilizing mechanism, which in its simplest form leads to the well-known Kelvin–Helmholtz (K-H) instability. This instability operates in stratified shear flows, provided the stratification is not too strong. The instability causes certain perturbations (i.e. instability modes) to amplify exponentially. Once reaching an appreciable amplitude, they evolve nonlinearly to form complex structures, such as vortex billows.

One of the most important stratified shear flows in nature is the atmospheric boundary layer, which occupies the lowest portion of the atmosphere (about 100 m to a few km) (Stull 1988). The flow field in this layer is strongly and directly influenced by the surface in order to satisfy the no-slip boundary condition. During the daytime, the rapid temperature rise near the ground means that vigorous convection takes place, rendering the flow fully turbulent. However, stratification reverts to a stable state during the night, and consequently the nocturnal boundary layer is characterized by intermittent bursts of turbulence, interspersed by periods of laminar, but highly unsteady, fluctuations (Coulter & Doran 2002; Nakmura & Mahrt 2005).

The waves mentioned above have all been observed in the atmospheric boundary layer (Gossard & Hooke 1975), among which internal gravity waves are naturally the most prevalent (Chanin & Haucheccorne 1981; Einaudi, Bedard & Finnigan 1989). Major field studies are reported by Smith *et al.* (2002) and Smith (2003) on mountain lee waves, and by Newsom & Banta (2003) on shear instability waves. Nonlinear solitary waves represent yet another important form of waves. Two types of solitary waves have been observed in the atmosphere: those which propagate within the lower few kilometres of the troposphere, and those which extend over the entire troposphere. Usually, the former consist of several waves of elevation (a spectacular example of which is the well-known 'morning glory' phenomenon), whereas the latter correspond to isolated waves of depression (for reviews, see Smith 1988; Christie 1989; Rottman & Grimshaw 2002).

All these waves are closely related to a range of atmospheric boundary-layer phenomena that have important meteorological implications. For instance, nocturnal boundary-layer intermittency occurs because of both the intrinsic boundary-layer instability and triggering by external disturbances. Recent field observations have identified the latter to be internal gravity waves, solitary waves (which may be a specific form of internal waves) (Sun *et al.* 2004) and density currents originating from distant sources (Sun *et al.* 2002). Weak turbulence in nocturnal boundary layers also implies that waves play a predominant role in transporting moisture and heat away from the surface, as well as in transporting momentum to the surface. Mountain lee waves may cause orographic wind storms (Lilly & Zipser 1972) and severe clear-air turbulence that can be hazardous to aircraft (Wurtele 1970; Ralph, Neiman & Levinson 1997). Mountain lee waves and internal gravity waves in general exert a mean drag on the tropospheric airflow, thereby influencing the circulation of the atmosphere (Lindzen 1981).

Various waves arise in the atmosphere, and can propagate horizontally over a long distance because the shear and stratification in the boundary layer act as a waveguide to trap the kinetic energy. Moreover, a shear flow often provides a source of energy, which feeds into waves via an instability mechanism (Drazin & Reid 1981).

Internal gravity waves and shear-instability waves can be treated in the same mathematical framework. Within linear and inviscid approximations, they are small perturbations superimposed on the background mean velocity and density profiles, and are governed by the Taylor–Goldstein equation (Goldstein 1931; Taylor 1931) together with appropriate boundary conditions. Such a boundary-value problem can be solved to predict the development and propagation of the waves, including the dispersion relation, the growth rate and the vertical distribution of the wave energy (Gossard & Hooke 1975). In the presence of shear, the distinction between gravity and shear-instability waves becomes blurred. If we insist that gravity waves must be a continuation of the waves that exist in shear-free situation, then only those which do not extract energy from the background shear flow can be called gravity waves,

i.e. they must correspond to a class of neutrally stable modes. Discrete modes of this kind arise only in some special cases, and so gravity waves consist primarily of the continuous spectrum of the Taylor–Goldstein equation. Shear-instability waves correspond to those modes which amplify at the expense of the mean-flow energy. They are usually trapped in the shear layer, except the long-wavelength modes, which may decay very slowly in the transverse direction and thus appear to be radiating in practice. In most of the literature on atmospheric science, however, the above distinction is not strictly made. Rather it is customary to refer loosely to the short-wavelength portion of the spectrum of the Taylor–Goldstein equation as (K-H) shear instability waves and the long-wavelength band as gravity waves (e.g. Lalas & Einaudi 1976; Mastrantonio *et al.* 1976; Chimonas 2002).

The dynamic stability of a stratified flow is controlled by the Richardson number Ri, which measures the relative importance of the stabilizing effect of density stratification to the destabilizing effect of the shear. A useful general result is that a necessary (but not sufficient) condition for inviscid shear instability to occur is that the Richardson number Ri must be less than 1/4 somewhere in the flow (Howard 1961; Miles 1961; Chimonas 1970). This criterion provides a quick assessment of the possibility of an inviscid instability. Analytical solutions of the Taylor–Goldstein equation can be found only for some special velocity and temperature distributions (Drazin & Howard 1966; Gossard & Hooke 1975). In general, the equation must be solved numerically. This has been carried out by a number of investigators for profiles pertaining to atmospheric conditions (e.g. Davis & Peltier 1976; Lalas, Einaudi & Fua 1976; Mastrantonio *et al.* 1976; Merrill 1977). The theoretical results were found to correlate reasonably well with the observed waves. Dominant instability modes have wavelengths comparable with the width of the background shear layer, and they primarily concentrate in the so-called critical layer, i.e. a thin region surrounding the level at which the base-flow velocity is equal to the phase speed. The wave momentum flux is usually weak, and there is little momentum/energy transport across the critical layer. The instability property depends on the profiles used (Mastrantonio *et al.* 1976; Chimonas & Grant 1984) and can be significantly altered by the presence of the ground. The latter may induce long-wavelength modes even at finite values of Ri (Davis & Peltier 1976; Lalas & Einaudi 1976; Mastrantonio *et al.* 1976). It may be noted that in all these studies except that of Mastrantonio *et al.* (1976), the base flows have a non-zero velocity at the ground, which means that the models may not have fully accounted for the ground effect.

Mountain waves are essentially stationary gravity waves excited by topography. The mathematical prediction of such wave fields was initiated by Queney (1948) and Scorer (1949). Viscosity and turbulence were both ignored, and no boundary layer was present. Such an inviscid laminar-flow approximation was followed in many subsequent studies. Theories which take into account turbulence and viscous effects have been developed since the 1970s, and a vast literature has accumulated. Wood (2000) reviews the technical and historical developments. Here, it suffices to mention the work of Sykes (1978), who adapted the well-known triple-deck theory (Smith 1973; Stewartson 1974) to describe the atmospheric flow past a mountain. The height and the horizontal scale of the mountain were chosen such that the local flow is described by the standard triple-deck structure, consisting of a lower deck, where the flow is viscous and nonlinear, a main deck, where the flow is rotational but inviscid, and an inviscid upper deck. The viscous motion produces a displacement, which is transmitted across the main deck and converted to a normal velocity. The latter induces in the upper deck a pressure gradient which in turn acts on the viscous lower

deck. The whole system is therefore interactive and the pressure is part of the solution. As such, the theory can accommodate a zone of separated flow. The solution also shows that lee waves are generated in the upper deck. The theory was later extended to three-dimensions (Sykes 1980). Formulated for a laminar and somewhat idealized background flow, this approach seems to be the only fully consistent viscous theory for mountain flows/waves, and it will form the basis of the present investigation.

Solitary waves have localized profiles, which retain their shapes during propagation because of the balance between the nonlinear steepening and linear dispersion effects. These waves originate from strong disturbances, such as a thunderstorm outflow or sea breezes, perturbing the background stably stratified shear layer. Most theories for such nonlinear waves have been developed based on the two basic assumptions that (*a*) the wavelengths are much longer than the thickness of the stratified shear layer, and (*b*) the waves are weakly nonlinear, i.e. the displacement amplitude of the waves is much smaller than the characteristic width of the shear layer. The shear layer serves as a horizontal waveguide to provide energy trapping. The lower boundary of the waveguide is the Earth's surface, whereas the upper boundary is either an infinitely deep layer of homogeneous fluid or a rigid lid. The former boundary condition leads to the well-known Benjamin–Davis–Ono (BDO) equation (Benjamin 1967; Davis & Acrivos 1967; Ono 1975; Grimshaw 1981), whereas the latter leads to the Kortweg–de Vries (KdV) equation (Benney 1966; Gear & Grimshaw 1983; Maslowe & Redekopp 1980). The particular applications to atmospheric solitary waves have been described, for example in Rottman & Einaudi (1993) and Rottman & Grimshaw (2002).

Most previous studies were concerned with inviscid instabilities. However, the relevance of possible viscous instabilities cannot be discarded. First, waves which have much longer wavelengths and periods than those of K-H modes have frequently been observed in the first tens to hundreds of metres of the atmosphere (e.g. Caughey & Reading 1975; Einaudi *et al.* 1989). Unlike K-H modes, these waves tend to carry strong momentum flux (Eymard & Weill 1979). Although long-wavelength invsicid modes do arise in the presence of the ground (e.g. Davis & Peltier 1976; Mastrantonio *et al.* 1976), their significance is undermined by their extremely small growth rates, which may be further reduced by viscous dissipation (Davis & Peltier 1977). Secondly, waves are often observed in atmospheric boundary layers whose velocity profiles do not have an inflection point. Although the presence of an inflection point is not a necessary condition for instability when a solid ground is present (Chimonas 1974), inflection-free profiles have often been found to be stable or very weakly unstable on the inviscid basis (Chimonas 2002). In these situations, it is of interest to look for alternative long-wavelength instability which has a viscous origin. The only work on possible viscous instability is that of Chimonas (1993, 1995), who showed that the aerodynamic surface drag acting on the surface layer may cause instability. The mathematical formulation was based on an empirical modelling of the surface friction (including both the molecular and Reynolds stresses), while the internal friction was ignored and the velocity in the surface layer was taken to be uniform.

In this paper, we investigate viscous instability of a stably stratified boundary layer, which is a modified form of the familiar Tollmien–Schlichting (T-S) waves. The instability problem will be formulated in § 2, and described in a self-consistent fashion using the well-known triple-deck theory (Smith 1979), adopted to take account of stratification. The general fully nonlinear system is presented in § 3. Linear spatial and temporal instabilities are considered in § 4. In § 5, we consider the high-frequency limit of the nonlinear system and derive a nonlinear evolution equation which is an extension of the BDO equation. The equation is solved numerically. In § 6, we show

that for a jet-like profile with small but non-zero free-stream velocity, the triple-deck theory must be adjusted to take into account the displacement and the normal pressure gradient induced by the inviscid motion in the main deck. The nonlinear evolution of high-frequency disturbances in such a flow is shown to be governed by a mixed KdV-BDO equation. A summary and some concluding remarks are given in § 7.

The coupling of the viscous instability waves with gravity waves will be considered in Part 2 (Wu & Zhang 2008).

2. Statement of the problem and formulation

We consider a two-dimensional boundary layer which forms owing to a uniform flow over flat terrain. The flow is assumed to be incompressible, and the usual Boussinesq approximation is invoked to account for the effect of density stratification on the dynamics. In the Cartesian coordinates (x^*, y^*), with x^* and y^* being the axes along and normal to the surface, respectively, the governing equations can be written, in the dimensional form, as

$$\frac{\partial u^*}{\partial t^*} + u^*\frac{\partial u^*}{\partial x^*} + v^*\frac{\partial u^*}{\partial y^*} = -\frac{1}{\bar{\rho}}\frac{\partial p^*}{\partial x^*} + \nu\nabla^2 u^*, \tag{2.1}$$

$$\frac{\partial v^*}{\partial t^*} + u^*\frac{\partial v^*}{\partial x^*} + v^*\frac{\partial v^*}{\partial y^*} = -\frac{1}{\bar{\rho}}\frac{\partial p^*}{\partial y^*} - \frac{g\rho^*}{\bar{\rho}} + \nu\nabla^2 v^*, \tag{2.2}$$

$$\frac{\partial \rho^*}{\partial t^*} + u^*\frac{\partial \rho^*}{\partial x^*} + v^*\frac{\partial \rho^*}{\partial y^*} = \kappa\nabla^2 \rho^*, \tag{2.3}$$

$$\frac{\partial u^*}{\partial x^*} + \frac{\partial v^*}{\partial y^*} = 0, \tag{2.4}$$

where t^* is the dimensional time, (u^*, v^*) and p^* denote the velocity and pressure, respectively, and ρ^* is the density variation from the mean density $\bar{\rho}$; an asterisk indicates a dimensional variable. Here ν and κ stand for the kinematic viscosity and thermal diffusivity, respectively, and g is the acceleration due to gravity.

We are interested in how the well-known viscous T-S instability is modified by stratification. In addition to being a problem of fundamental interest in itself, it may be relevant to certain long waves which reside in the so-called low-level jet occupying the first few hundred metres of the atmosphere. The effect of the rotation is excluded from the formulation for simplicity. In the intended application, the waves of interest have periods of about 10 min (e.g. Einaudi *et al.* 1989; Sun *et al.* 2004), which is sufficiently short that the Coriolis force can be neglected.

Suppose that at the location of interest, the boundary layer has a local thickness δ and a characteristic velocity U_0. Then we can define a local Reynolds number

$$R = U_0\delta/\nu, \tag{2.5}$$

which is assumed to be large, i.e. $R \gg 1$.

The effect of stratification is characterized by a local inverse internal Froude number

$$S = N\delta/U_0, \tag{2.6}$$

where N is the local Brunt–Väisälä frequency, defined as

$$N = (-(g/\bar{\rho})\mathrm{d}\rho_0^*/\mathrm{d}y^*)^{1/2}, \tag{2.7}$$

with $\rho_0^*(y^*)$ being the basic density profile. In this study, we shall assume that N is constant, that is, the density varies with y^* linearly. This restriction can be somewhat relaxed; see the discussion in § 3.1.

Introduce non-dimensionalized variables by writing

$$(x^*, y^*) = \delta(x, y), \quad t^* = t\delta/U_0, \quad (u^*, v^*) = U_0(u, v), \quad p^* = \bar{\rho}U_0^2 p. \tag{2.8}$$

The basic density ρ_0^* can be eliminated from (2.2) by absorbing the hydrostatic pressure P_0^*, defined by $\mathrm{d}P_0^*/\mathrm{d}y^* = -g\rho_0^*$, into the pressure p^*. Then the buoyancy term in (2.2) becomes $-(g/\bar{\rho})(\rho^* - \rho_0^*)$, which in turn can be re-written as $-\delta N^2\rho$ once a dimensionless density fluctuation (Sykes 1978),

$$\rho = (\rho^* - \rho_0^*)/(-\delta \mathrm{d}\rho_0^*/\mathrm{d}y^*), \tag{2.9}$$

is introduced. Equation (2.3) can be rewritten in terms of ρ. The full dimensionless equations become

$$\frac{\partial u}{\partial t} + u\frac{\partial u}{\partial x} + v\frac{\partial u}{\partial y} = -\frac{\partial p}{\partial x} + \frac{1}{R}\nabla^2 u, \tag{2.10}$$

$$\frac{\partial v}{\partial t} + u\frac{\partial v}{\partial x} + v\frac{\partial v}{\partial y} = -\frac{\partial p}{\partial y} - S^2\rho + \frac{1}{R}\nabla^2 v, \tag{2.11}$$

$$\frac{\partial u}{\partial x} + \frac{\partial v}{\partial y} = 0, \tag{2.12}$$

$$\frac{\partial \rho}{\partial t} + u\frac{\partial \rho}{\partial x} + v\frac{\partial \rho}{\partial y} - v = \frac{1}{Pr\,R}\nabla^2\rho, \tag{2.13}$$

where Pr is the Prandtl number, and S characterizes the stratification effect.

In the context of the atmospheric boundary layer, the background basic flow $(U_B, R^{-1}V_B)$ may have rather complex profiles, depending on meteorological conditions. Indeed, the flow is often turbulent. A steady laminar base flow will be assumed in the present study, since our main interest is in waves in nocturnal boundary layers, which are in a more-or-less laminar state, interrupted by brief outbursts of intermittent turbulence (Nakmura & Mahrt 2005). Moreover, we shall assume that $U_B(y)$ is such that

$$U_B \sim \lambda y, \quad \text{as} \quad y \to 0, \quad U_B \sim u_\infty \quad \text{as} \quad y \to \infty, \tag{2.14}$$

with $\lambda = O(1)$ and u_∞ being 'constants'. The function $U_B(y)$ is an otherwise arbitrary function of y and does not have to be monotonic. As usual, the horizontal slow variation on the scale $x \sim O(R)$ is suppressed, which is justified since the waves to be considered have length scales much shorter than $O(R)$.

Two representative cases will be considered. The first corresponds to $u_\infty = O(1)$. The second case has $u_\infty \ll 1$, which is characteristic of low-level jets and tropospheric jet streams (Mastrantonio *et al.* 1976). Specifically, we consider $u_\infty = O(R^{-1/7})$, which is a distinguished scaling for reasons that will become clear later (§ 6).

In order to study the stability of the base flow, a small perturbation is introduced so that the total flow field can be written as

$$(u, v, p, \rho) = (U_B, R^{-1}V_B, P_B, 0) + (\tilde{u}, \tilde{v}, \tilde{p}, \tilde{\rho}), \tag{2.15}$$

where the mean pressure P_B in general is non-uniform. The characteristic scalings of the instability modes are different for the cases $u_\infty = O(1)$ and $u_\infty = O(R^{-1/7})$. These will be considered in turn.

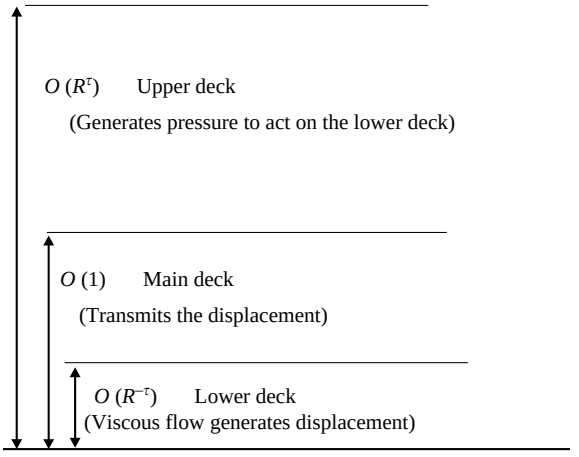

FIGURE 1. Triple-deck structure: the width and main role of each deck. For $u_\infty = O(1)$, $\tau = 1/4$ (cf. Smith 1979). For a jet-like profile with $u_\infty = O(R^{-1/7})$, $\tau = 1/7$ (cf. Smith & Duck 1977).

3. The triple-deck structure with stratification effect

3.1. *Triple-deck scaling*

For the case $u_\infty = O(1)$, the viscous instability is a modified form of the T-S waves in a boundary layer. The unstable modes have characteristic wavelength and frequency of $O(R^{1/4}\delta)$ and $O(R^{-1/2}U_0/\delta)$, respectively, and so we introduce the scaled spatial and temporal variables

$$X = R^{-1/4}x \equiv \epsilon x, \quad T = R^{-1/2}t \equiv \epsilon^2 t, \tag{3.1}$$

where

$$\epsilon = R^{-1/4}. \tag{3.2}$$

The instability can be described by the standard triple-deck structure (Smith 1979), consisting of a main deck where $y \sim O(1)$, an upper deck where $y \sim R^{1/4}$, and a lower deck where $y \sim R^{-1/4}$ (see figure 1). This structure remains intact for weak stratifications corresponding to $S \sim O(\epsilon)$, as was realized by Sykes (1978). Thus, S is scaled as

$$S = \epsilon s, \tag{3.3}$$

for which the buoyancy term is a leading-order effect in the upper deck, but largely negligible in the main and lower decks. As indicated by (3.1), the viscous instability modes have asymptotically large wavelengths, and low frequencies or correspondingly small phase speeds.

Before turning to mathematical details, let us discuss the implications of the assumptions of a weak stratification ($S \ll O(1)$) and a linear density profile ($S =$ constant). From (2.6) and (2.7) it follows that $S \ll O(1)$ corresponds to

$$(\Delta y^*/\delta)/(\Delta\rho^*/\bar{\rho}) \gg g\delta/U_0^2, \tag{3.4}$$

where $\Delta\rho^*$ denotes the density variation (from a reference value $\bar{\rho}$ over a vertical distance Δy^*). For the stratification effect to be present in the upper deck, it is required that $\Delta y^*/\delta \gg O(1)$, i.e. the density variation occurs over a length scale much greater than the boundary-layer thickness, but the relative variation $\Delta\rho^*/\bar{\rho}$ may be of order one or smaller. The flow stability is affected, to leading order, by the density

profile at the outer edge of the boundary layer, while its distribution in the main deck is largely irrelevant since stratification does not play a leading role there. Therefore, the present theory is not restricted to a globally linear stratification of density; it is actually applicable to more general density profiles provided they approach a linear asymptote in the far field. A linear temperature profile at the outer edge of the boundary layer was generated in laboratory conditions (Ohya & Uchida 2003). It has also been observed in nocturnal atmospheric boundary layers, where intermittent turbulence occurs (see e.g. figure 4 of Newsom & Banta 2003). In both cases, the relative change in temperature is fairly small, and it thus can be deduced from a Taylor expansion of the density–temperature relation that the density in the outer reach of the boundary layer must also vary linearly with the height.

In passing, we note that using triple-deck formalism, Mureithi (1997) studied the effect of unstable stratification on low-branch T-S waves, while its influence on the upper branch instability was considered in Mureithi, Denier & Stott (1997). In both studies, the density (temperature) variation is assumed to be confined within the boundary layer. As a result, the free stream is homogeneous and hence supports no gravity waves, and the stability is affected only when stratification is strong enough for buoyancy to manifest itself in the main deck. In contrast, in our study, the density varies across a vertical depth much thicker than the boundary layer. Gravity waves can be present in the free stream, and a weak stratification over such a long scale can influence the stability.

3.2. *The main deck*

In the main deck, where $y = O(1)$, the perturbation takes the form

$$(\tilde{u}, \tilde{v}, \tilde{p}, \tilde{\rho}) = (\epsilon U_1, \epsilon^2 V_1, \epsilon^2 P_1, \epsilon\rho_1) + \cdots. \tag{3.5}$$

Here the magnitude of the perturbation is chosen such that the lower deck is fully nonlinear. This leads to a general formulation, which can be subsequently linearized for smaller disturbances. It follows from substituting (2.15) with (3.5) into (2.10)–(2.13) and using (3.1) that (U_1, V_1, P_1, ρ_1) satisfy equations (cf. Stewartson 1974)

$$\frac{\partial U_1}{\partial X} + \frac{\partial V_1}{\partial y} = 0, \quad U_B \frac{\partial U_1}{\partial X} + U_B' V_1 = 0, \quad U_B \frac{\partial \rho_1}{\partial X} = V_1, \quad \frac{\partial P_1}{\partial y} = 0.$$

The velocity and density has the solution

$$U_1 = A(X, T) U_B', \quad V_1 = -A_X U_B, \quad \rho_1 = -A(X, T). \tag{3.6}$$

The pressure does not vary across the main deck so that

$$P_1 = P(X, T), \tag{3.7}$$

where A and P are arbitrary functions of X and T.

3.3. *The upper deck*

The transverse variable in the upper deck is $\tilde{y} = \epsilon y$, and the perturbation expands as

$$(\tilde{u}, \tilde{v}, \tilde{p}, \tilde{\rho}) = (\epsilon^2 \hat{U}, \epsilon^2 \hat{V}, \epsilon^2 \hat{P}, \epsilon\hat{\rho}) + \cdots. \tag{3.8}$$

Then substituting (2.15) along with (3.8) into (2.10)–(2.13) yields

$$u_\infty \frac{\partial \hat{U}}{\partial X} = -\frac{\partial \hat{P}}{\partial X}, \tag{3.9}$$

$$u_\infty \frac{\partial \hat{V}}{\partial X} = -\frac{\partial \hat{P}}{\partial \tilde{y}} - s^2 \hat{\rho}, \tag{3.10}$$

$$\frac{\partial \hat{U}}{\partial X} + \frac{\partial \hat{V}}{\partial \tilde{y}} = 0, \tag{3.11}$$

$$u_\infty \frac{\partial \hat{\rho}}{\partial X} = \hat{V}. \tag{3.12}$$

By eliminating $\hat{U}$, $\hat{V}$ and $\hat{\rho}$ among these equations, it can be deduced that

$$\frac{\partial^2 \hat{P}}{\partial X^2} + \frac{\partial^2 \hat{P}}{\partial \tilde{y}^2} + \hat{s}^2 \hat{P} = 0, \tag{3.13}$$

where we have put

$$\hat{s} = s/|u_\infty|.$$

By taking the limit $\tilde{y} \to 0$ in (3.10), and matching with the large-y asymptote of the main-deck solution (3.6), we find the boundary condition

$$\frac{\partial \hat{P}}{\partial \tilde{y}} = u_\infty^2 (A_{XX} + \hat{s}^2 A) \quad \text{at} \quad \tilde{y} = 0. \tag{3.14}$$

Now (3.13) with (3.14) forms a Neumann boundary-value problem for a Helmholtz equation. It can be solved by taking the Fourier transform with respect to X, as in Maslowe & Redekopp (1980) and Romanova (1981). Let $\hat{p}$ and $\hat{a}$ denote the Fourier transforms of $\hat{P}$ and A, respectively. Then

$$\hat{p} = -\mathrm{i}m\,\hat{a} u_\infty^2 \mathrm{e}^{\mathrm{i}m\tilde{y}} \quad \text{with} \quad m = (\hat{s}^2 - k^2)^{1/2}, \tag{3.15}$$

where the branch of m is chosen to ensure that its imaginary part is positive if m is complex, and that $m \geqslant 0$ (< 0) if it is real and $0 < k < \hat{s}$ ($-\hat{s} < k < 0$). This follows from the requirement that the pressure perturbation in the upper deck must either decay exponentially or represent a radiating (gravity) wave. Clearly, an m with a positive imaginary part guarantees an exponential decay. On the other hand, a positive (negative) m for $k > 0$ ($k < 0$) gives a positive vertical group velocity so that the disturbance is outgoing (Sykes 1978; Maslowe & Redekopp 1980; Romanova 1981). Putting $\tilde{y} = 0$ in (3.15) yields the pressure–displacement relation in spectral space

$$\hat{p} = -\mathrm{i}m\,\hat{a} u_\infty^2. \tag{3.16}$$

This can be inverted by using the convolution theorem to obtain the pressure–displacement relation in physical space

$$P(X, T) = u_\infty^2 \int_{-\infty}^{\infty} \mathscr{G}(X;\xi)(A_{\xi\xi}(\xi, T) + \hat{s}^2 A(\xi, T))\mathrm{d}\xi, \tag{3.17}$$

where

$$\begin{aligned} \mathscr{G}(X;\xi) &= \tfrac{1}{2}\{Y_0(\hat{s}|X-\xi|) + \boldsymbol{H}_0(\hat{s}(X-\xi))\} \\ &\equiv \tfrac{1}{2}\Big\{-\frac{2}{\pi}\int_{\hat{s}}^{\infty} \frac{\cos \hat{s}(X-\xi)}{\sqrt{k^2 - \hat{s}^2}}\mathrm{d}k + \frac{2}{\pi}\int_0^{\hat{s}} \frac{\sin \hat{s}(X-\xi)}{\sqrt{\hat{s}^2 - k^2}}\mathrm{d}k\Big\} \end{aligned} \tag{3.18}$$

with Y_0 being the order-one Bessel function of the first kind, $\boldsymbol{H}_0$ being the order-one Struve function. Here the integral should be interpreted as a Cauchy principal value.

3.4. *The lower deck*

In the lower deck, the appropriate transverse coordinate is defined by

$$Y = y/\epsilon. \tag{3.19}$$

The disturbance can no longer be treated as a small perturbation because it has a magnitude comparable with the base flow velocity. The total flow field takes the form

$$(u, v, p, \rho) = \epsilon(U, \epsilon^2 V, \epsilon P, \rho) + \cdots, \tag{3.20}$$

Substitution of the above expansion into (2.10)–(2.13) yields, at leading order,

$$\frac{\partial U}{\partial T} + U\frac{\partial U}{\partial X} + V\frac{\partial U}{\partial Y} = -\frac{\partial P}{\partial X} + \frac{\partial^2 U}{\partial Y^2}, \tag{3.21}$$

$$\frac{\partial U}{\partial X} + \frac{\partial V}{\partial Y} = 0, \tag{3.22}$$

plus $\partial P/\partial Y = 0$, which has been used to equate the pressure in the lower deck to $P(X, T)$. On the ground, U and V satisfy the no-slip and no-penetration boundary conditions, i.e.

$$U = V = 0 \quad \text{at} \quad Y = 0, \tag{3.23}$$

while matching ϵU with $(U_B + \epsilon U_1)$ in the main deck (see (3.6)) requires

$$U \to \lambda(Y + A(X, T)) \quad \text{as} \quad Y \to \infty. \tag{3.24}$$

The nonlinear instability problem is described by the system consisting of equations (3.21)–(3.22), the pressure–displacement relation (3.17), and the boundary and matching conditions (3.23) and (3.24).

Note that since the streamwise velocity of the disturbance is of the same order of magnitude, viscous T-S modes spread over the majority of the boundary layer, in contrast to typical K-H modes, which concentrate in their critical layers.

4. Linear stability analysis

4.1. *Derivation of the dispersion relation*

Now we assume that the perturbation is weak, i.e. $(V, P, A) = O(\tilde{\epsilon})$ with $\tilde{\epsilon} \ll 1$. Then the streamwise velocity U in the lower deck is a uniform shear flow λY superimposed by a small perturbation. We thus can write

$$(U, V, A, P) = (\lambda Y, 0, 0, 0) + \tilde{\epsilon}(\tilde{u}_s, \tilde{v}_s, \tilde{a}_s, \tilde{p}_s) + \cdots. \tag{4.1}$$

Substituting (4.1) into (3.21)–(3.24) and linearizing for $\tilde{\epsilon} \ll O(1)$, we obtain

$$\frac{\partial \tilde{u}_s}{\partial T} + \lambda Y\frac{\partial \tilde{u}_s}{\partial X} + \lambda \tilde{v}_s = -\frac{\partial \tilde{p}_s}{\partial X} + \frac{\partial^2 \tilde{u}_s}{\partial Y^2}, \qquad \frac{\partial \tilde{u}_s}{\partial X} + \frac{\partial \tilde{v}_s}{\partial Y} = 0, \tag{4.2}$$

$$\tilde{u}_s = \tilde{v}_s = 0 \quad \text{at} \quad Y = 0; \quad \tilde{u}_s \to \lambda \tilde{a}_s \quad \text{as} \quad Y \to \infty, \tag{4.3}$$

supplemented by the pressure–displacement relation, which remains as (3.17) with P and A being replaced by $\tilde{p}_s$ and $\tilde{a}_s$, respectively.

We can seek normal modes of the travelling-waveform

$$(\tilde{u}_s, \tilde{v}_s, \tilde{a}_s, \tilde{p}_s)) = (\hat{u}_s, \hat{v}_s, \hat{a}_s, \hat{p}_s)\mathrm{e}^{\mathrm{i}(kX - \omega T)} + \text{c.c.}$$

Then $(\hat{u}_s, \hat{v}_s, \hat{a}_s, \hat{p}_s)$ satisfy the equations

$$-\mathrm{i}\omega\hat{u}_s + \mathrm{i}k\lambda Y\hat{u}_s + \lambda\hat{v}_s = -\mathrm{i}k\hat{p}_s + \hat{u}_s'', \tag{4.4}$$

$$\mathrm{i}k\hat{u}_s + \hat{v}_s' = 0, \tag{4.5}$$

$$\hat{u}_s = 0, \quad \hat{v}_s = 0 \quad \text{at} \quad Y = 0, \tag{4.6}$$

$$\hat{u}_s \to \lambda\hat{a}_s \quad \text{as} \quad Y \to \infty, \tag{4.7}$$

together with the pressure–displacement relation

$$\hat{p}_s = -\mathrm{i}m\hat{a}_s. \tag{4.8}$$

By differentiating (4.4) with respect to Y, and using (4.5) to eliminate $\hat{v}_s$, we have

$$\hat{u}_s''' - \mathrm{i}(k\lambda Y - \omega)\hat{u}_s' = 0. \tag{4.9}$$

The solution satisfying $\hat{u}_s = 0$ at $Y = 0$ is

$$\hat{u}_s = C\int_{\xi_0}^{\xi} \mathrm{Ai}(\xi)\mathrm{d}\xi, \tag{4.10}$$

where C is a constant, Ai denotes the Airy function, and

$$\xi = (\mathrm{i}k\lambda)^{1/3}Y + \xi_0, \qquad \xi_0 = -\mathrm{i}\omega(\mathrm{i}k\lambda)^{-2/3}. \tag{4.11}$$

The vertical velocity can be found from (4.5),

$$\hat{v}_s = -\mathrm{i}k(\mathrm{i}k\lambda)^{1/3}C\int_{\xi_0}^{\xi}(\xi - \tilde{\xi})\mathrm{Ai}(\tilde{\xi})\mathrm{d}\tilde{\xi}. \tag{4.12}$$

From the matching requirement (4.7), it follows that

$$C\int_{\xi_0}^{\infty} \mathrm{Ai}(\xi)\mathrm{d}\xi = \lambda\hat{a}_s. \tag{4.13}$$

Setting $Y = 0$ in (4.4) yields $\hat{u}_s''(\xi_0) = \mathrm{i}k\hat{p}_s$. Application of this gives

$$C\mathrm{Ai}'(\xi_0)(\mathrm{i}k\lambda)^{2/3} = \mathrm{i}k\hat{p}_s. \tag{4.14}$$

Elimination of $\hat{p}_s$ and $\hat{a}_s$ among (4.8) and (4.13)–(4.14) leads to the dispersion relation

$$\Delta(k, \omega) \equiv \int_{\xi_0}^{\infty} \mathrm{Ai}(\xi)\mathrm{d}\xi - \lambda(\mathrm{i}k\lambda)^{2/3}\mathrm{Ai}'(\xi_0)/(km) = 0. \tag{4.15}$$

When $\hat{s} = 0$, (4.15) is just the lowest-order large-R asymptotic approximation to the characteristic equation for the lower branch T-S waves (Smith 1979).

4.2. *Spatial and temporal growth rates*

From (4.15), we can calculate either the complex wavenumber $k = k_r + \mathrm{i}k_i$ for a given real ω (spatial instability), or the complex frequency $\omega = \omega_r + \mathrm{i}\omega_i$ for a given real wavenumber k (temporal instability). For that purpose, it is necessary to evaluate the Airy function $\mathrm{Ai}(\xi)$ numerically. This was done by a fourth-order Runge–Kutta method, starting from a large ξ, at which the initial values are given by the asymptotic behaviours of Ai and Ai′ (Abramowitz & Stegun 1964),

$$\mathrm{Ai}(\xi) \sim \tfrac{1}{2}\pi^{-1/2}\xi^{-1/4}\mathrm{e}^{-\zeta}\sum_{0}^{\infty}(-1)^n c_n\zeta^{-n}, \tag{4.16}$$

$$\mathrm{Ai}'(\xi) = -\tfrac{1}{2}\pi^{-1/2}\xi^{1/4}\mathrm{e}^{-\zeta}\sum_{0}^{\infty}(-1)^n d_n\zeta^{-n}, \tag{4.17}$$

where $\zeta = (2/3)\xi^{3/2}$, and the constants are defined by

$$c_0 = 1, \quad c_k = \frac{\Gamma\left(3k+\frac{1}{2}\right)}{54^k k!\Gamma\left(k+\frac{1}{2}\right)}; \quad d_0 = 1, \quad d_k = -\frac{6k+1}{6k-1}c_k, \tag{4.18}$$

with $\Gamma(k)$ being the gamma function. The root of the dispersion relation is sought by Newton–Raphson iteration. Numerical results will be presented below.

In conjunction with numerical results, approximations can be found in the high-frequency (or short-wavelength) limit, corresponding to $k, \omega \gg O(1)$. It turns out that ω is $O(k^2)$ (see below) so that $\xi_0 = O(k^{4/3}) \gg O(1)$, for which (Abramowitz & Stegun 1964)

$$\int_{\infty}^{\xi_0} \mathrm{Ai}(\xi)\mathrm{d}\xi = -\tfrac{1}{2}\pi^{-1/2}\xi_0^{-3/4}\exp\left(-\tfrac{2}{3}\xi_0^{3/2}\right)\left[1-\left(\tfrac{3}{4}+\tfrac{3}{2}c_1\right)\xi_0^{-3/2}+O\left(\xi_0^{-3}\right)\right]. \tag{4.19}$$

On using (4.17) and (4.19) in (4.15), the dispersion relation is approximated by

$$k\left[1-\left(\tfrac{3}{4}+\tfrac{3}{2}c_1\right)\xi_0^{-3/2}+O\left(\xi_0^{-3}\right)\right]+\lambda(\mathrm{i}k\lambda)^{2/3}\xi_0\frac{1}{\sqrt{\hat{s}^2-k^2}}\left[1-\tfrac{3}{2}d_1\xi_0^{-3/2}+O\left(\xi_0^{-3}\right)\right]=0. \tag{4.20}$$

Consider temporal instability first, for which k is real. We assume that $k \sim \hat{s} \gg 1$, and an inspection of the balance in (4.20) suggests that ω expands as

$$\omega = k^2(\omega_0 + k^{-2}\omega_1 + \cdots). \tag{4.21}$$

Inserting (4.21) into (4.20), we found that for $k < \hat{s}$

$$\left.\begin{aligned}\omega_0 &= -\frac{\mathrm{i}}{\lambda}(\hat{s}^2/k^2-1)^{1/2},\\ \omega_1 &= \mathrm{i}\left(\tfrac{3}{4}+\tfrac{3}{2}c_1-\tfrac{3}{2}d_1\right)(\hat{s}^2/k^2-1)^{-1/4}\lambda^{3/2} = \mathrm{i}(\hat{s}^2/k^2-1)^{-1/4}\lambda^{3/2}.\end{aligned}\right\} \tag{4.22}$$

The above expressions are also valid for $k > \hat{s}$ provided the branch of the square root is taken to be $\mathrm{e}^{\mathrm{i}\pi/2}(1-\hat{s}^2/k^2)^{1/2}$, yielding

$$\left.\begin{aligned}\omega_0 &= \frac{1}{\lambda}(1-\hat{s}^2/k^2)^{1/2},\\ \omega_1 &= \mathrm{e}^{\pi\mathrm{i}/4}(1-\hat{s}^2/k^2)^{-1/4}\lambda^{3/2}.\end{aligned}\right\} \tag{4.23}$$

The results (4.22) and (4.23) indicate that the modes within the band $1 \ll k < \hat{s}$ are highly damped, while those in the band $k > \hat{s}$ are nearly neutral. Both (4.22) and (4.23), however, cease to be valid when $(1-\hat{s}^2/k^2) \sim O(k^{-8/3})$ because expansion (4.21) becomes disordered. Furthermore, since ω becomes $O(k^{2/3})$, $\xi_0 = O(1)$ and so (4.17) and (4.19) can no longer be used. The full dispersion relation (4.15) must be solved. Nevertheless, the above consideration suggests that the most unstable mode exists in this regime, in which the real and imaginary parts of ω are comparable, both of $O(k^{2/3})$. Since $k \sim O(\hat{s})$, it follows that in the limit $\hat{s} \gg 1$, the most unstable mode has a characteristic frequency and a growth rate of $O(\hat{s}^{2/3})$. We therefore come to the surprising conclusion that stratification has a destabilizing effect in the present temporal instability formulation. Numerical solutions of the full dispersion relation will confirm this.

Consider now spatial instability, for which ω is real and can be taken to be positive without loss of generality. We assume that $\omega \gg 1$ and $\hat{s} \gg 1$ or more precisely $\hat{s} = O(\omega^{1/2})$ so that we can write

$$\hat{s} = \omega^{1/2}\hat{s}_0. \tag{4.24}$$

Inspection of the dominant balance in (4.20) suggests that k expands as

$$k = \omega^{1/2}(k_0 + \omega^{-1}k_1 + \cdots). \tag{4.25}$$

A straightforward calculation shows that

$$\left.\begin{aligned} k_0 &= \Big(\frac{\hat{s}_0^2 + \sqrt{\hat{s}_0^4 + 4\lambda^2}}{2}\Big)^{1/2}, \\ k_1 &= -\frac{\lambda^3}{\sqrt{\hat{s}_0^4 + 4\lambda^2}}\big(\tfrac{3}{4} + \tfrac{3}{2}c_1 - \tfrac{3}{2}d_1\big)\mathrm{e}^{\pi\mathrm{i}/4} = -\frac{\lambda^3 \mathrm{e}^{\pi\mathrm{i}/4}}{\sqrt{\hat{s}_0^4 + 4\lambda^2}}. \end{aligned}\right\} \tag{4.26}$$

The surface shear λ plays a key role in the present viscous instability. The dependence on it can be best elucidated by the scaling relations

$$k = \lambda^{5/4}k_N, \quad \omega = \lambda^{3/2}\omega_N, \quad \hat{s}_0 = \lambda^{5/4}\hat{s}_N. \tag{4.27}$$

It then follows that k_N and ω_N satisfy (4.15) with $\lambda = 1$ and s_N being the parameter. In the following, we shall present the result with $\lambda = 1$, but we shall drop the subscript 'N' for brevity.

Typical eigenvalues for temporal instability are shown in figure 2, where the frequency and growth rate, ω_r and ω_i, are plotted as functions of k for selected values of $\hat{s}$. Modes with small wavenumbers k (i.e. small frequencies ω_r) decay, whereas modes with relatively short wavelengths (i.e. large k) are unstable. As stratification becomes strong, a broader band of decaying modes become more severely damped (figure 2*b*). Meanwhile the unstable modes shift to the shorter wavelength end. Stratification tends to increase the maximum temporal growth rate. For the moderate values of $\hat{s}$ considered here, the growing modes are all trapped (i.e. with $k > \hat{s}$).

Figure 3 shows the temporal growth rates for two relatively large values of $\hat{s}$: $\hat{s} = 7$, 12. The numerical result obtained by solving the dispersion relation (4.15) is compared with the asymptotic approximation (4.21)–(4.22). The agreement is good even for moderate values of k. A close view of the band of growing modes is shown in figure 3(*b*). These modes locate to the right of $k = \hat{s}$, near which the maximum growth is attained. The maximum increases with $\hat{s}$, as suggested by the large-k asymptotic approximation. Only trapped modes ($k > \hat{s}$) are unstable, while radiating modes, i.e. those with $k < \hat{s}$, are heavily damped.

The numerical results together with the analysis in the limit $\hat{s} \gg 1$ indicate that stable stratification has a destabilizing effect for any value of $\hat{s}$. This is a surprising and highly counterintuitive result, despite the fact that a possible destabilizing role of stratification was implied previously in an example given by Thorpe (1969), who gave a velocity profile which is stable without stratification, but inviscidly unstable with stratification. The occurrence of instability in the later context may be understood in terms of an interaction between waves of negative and positive energies (Fabrikant & Stepanyants 1998). However, it does not seem possible to explain the present destabilization of viscous instability from that standpoint.

Figure 4 shows typical eigenvalues in the spatial instability formulation. Here the real (k_r) and imaginary (k_i) parts of the complex wavenumber are plotted as functions of frequency ω for selected values of $\hat{s}$. Consistent with the spatial instability result, modes with small ω are damped, and amplification occurs for relatively large ω. This means that if a perturbation is weak, it will decay initially. However, as it propagates downstream, its dimensionless frequency increases owing to the thickening of the boundary layer and thus the perturbation will eventually undergo amplification. Overall, stratification plays a stabilizing role in that the maximum growth rate

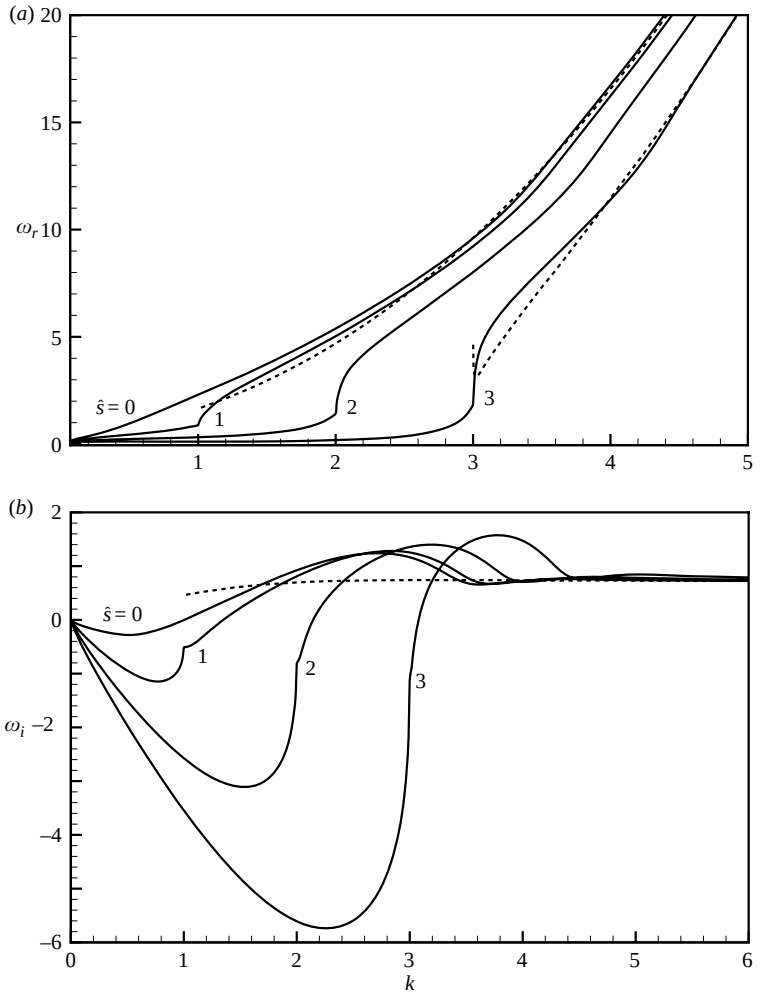

FIGURE 2. Temporal instability: eigenvalue ω *vs.* k for selected values of $\hat{s}$. (*a*) The real part (ω_r); (*b*) the imaginary part (ω_i). The dashed lines represent the asymptotic approximation (4.23).

decreases with $\hat{s}$. The stabilizing effect is not uniform for all disturbances as might be intuitively expected. For disturbances with frequencies in a certain range (e.g. $8 < \omega < 12$ in figure 4*b*), their local growth rates may be enhanced by moderate stratification (e.g. for $\hat{s} < 3$ in figure 4*b*). It is also surprising that stratification has opposite effects on the maximum growth rates in the temporal and spatial formulations.

4.3. *Relevance of viscous instability*

Waves in stratified boundary layers are usually attributed to inviscid instabilities of the K-H type. Possible viscous instability has received scant attention. The only viscous mechanism proposed is the drag-induced instability (Chimonas 1993, 1995). The present modified T-S instability represents another. The two viscous instabilities share the physics that viscous effect induces a suitable phase lag between the fluctuation of the velocity components in such a way that the resulting Reynolds stress feeds

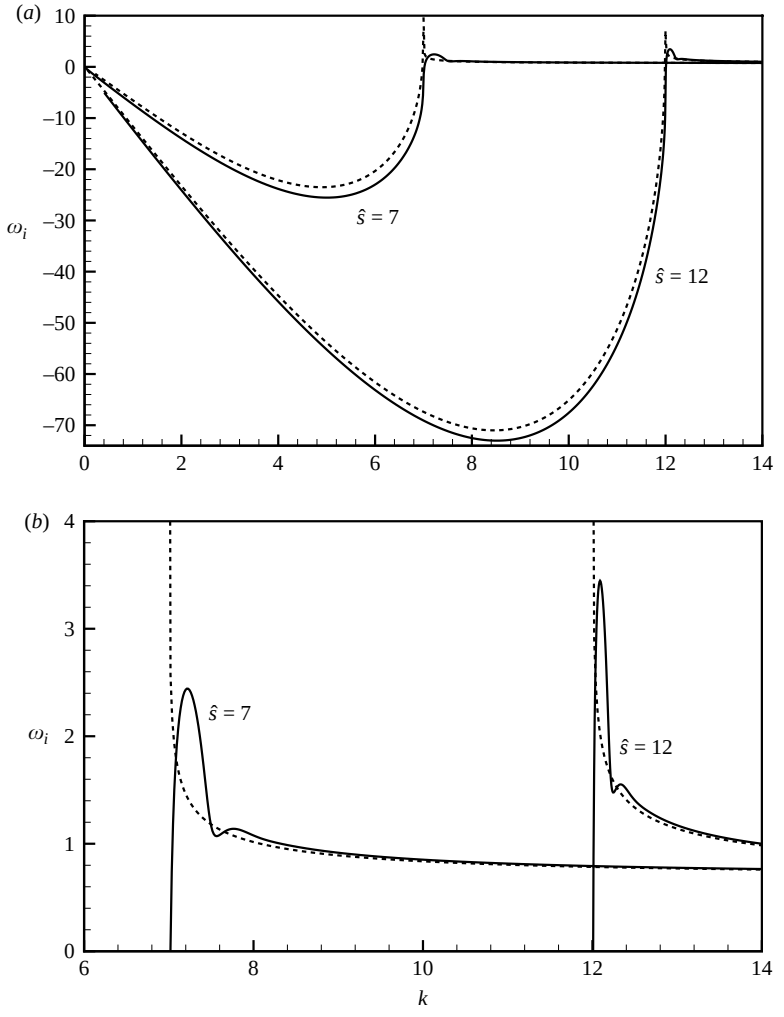

FIGURE 3. Temporal growth rate *vs.* wavenumber k for $\hat{s} = 7, 12$. The dotted lines represent the asymptotic approximation (4.22)–(4.23).

energy into the waves. However, the mathematical formulations are very different, and a concrete relation between them cannot be established.

The present paper shows that the T-S mechanism continues to operate in a stratified boundary layer, leading to amplification of waves whose wavelengths are much larger than the characteristic width of the shear layer. This viscous mechanism is complementary to K-H instability since the latter primarily amplifies relatively short-scale waves.

Evidence of T-S waves in stratified boundary layers can be found in the laboratory experiment of Ohya & Uchida (2003), who measured the fluctuations in the weak to strong stratification regimes. We performed the stability calculations pertaining to their weak stratification (i.e. S1) case, for which the measurement provided the velocity profile for $U_B(y) > 0.26$ (see their figure 2). Using the velocity data close to the wall, we deduced that the wall shear $\lambda \approx 3.0$, which is a rough estimate. A linear approximation was used to extrapolate the velocity from $U_B = 0.26$ to $U_B = 0$.

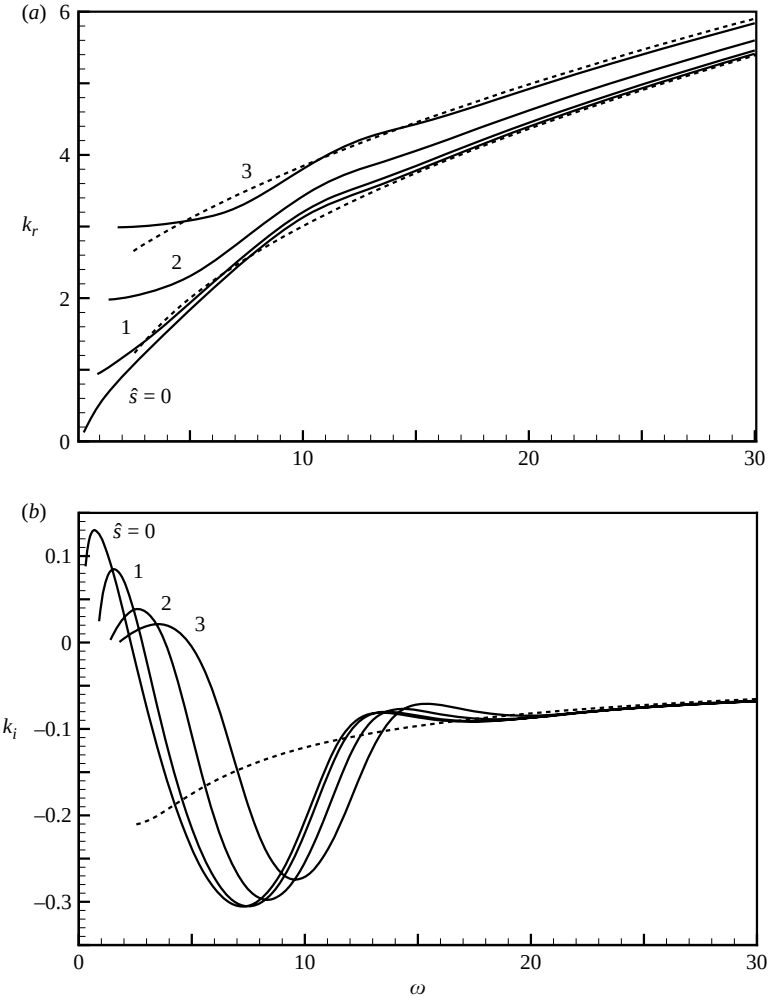

FIGURE 4. Spatial instability: the eigenvalue k *vs.* ω for selected values of $\hat{s}$. (*a*) The real part (k_r); (*b*) the imaginary part (k_i). The dashed lines represent the asymptotic approximation (4.26).

The origin of the vertical coordinate, corresponding to $U_B = 0$, was found to shift downward by 0.1δ.

At the location of measurement, the Reynolds number based on a nominal boundary-layer thickness $\delta = 0.45$ m is $R = 34500$. It follows that the small parameter $\epsilon = 6.92 \times 10^{-2}$. The Richardson number in the outer portion of the boundary layer is 0.28, from which we extracted a value for the stratification parameter $\hat{s} = 1.94$.

In order to facilitate a comparison with the experiment, we construct, using the multiplicative rule, a composite solution for the eigenfunction of the streamwise velocity,

$$\widehat{u}_c = U_B'(y) \int_{\xi_0}^{\xi} \mathrm{Ai}(\xi)\mathrm{d}\xi, \tag{4.28}$$

from the main-deck and lower-deck solutions, (3.6) and (4.10). Here a constant factor has been dropped from (4.28) since it does not affect the shape of the instability modes.

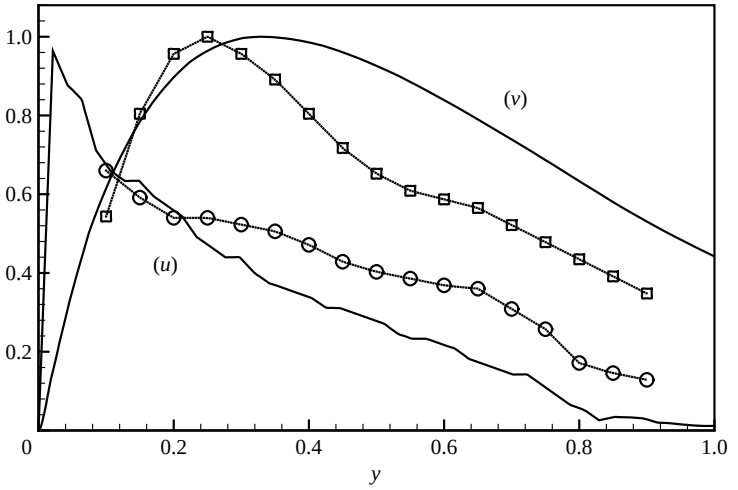

FIGURE 5. Comparison of the predicted mode shape (curves without symbols) for u and v with the experimental measurement (symbols) (Ohya & Uchida 2003).

Similarly, we obtain the composite solution for the vertical velocity component

$$\widehat{v}_c = \mathrm{e}^{\mathrm{i}m\tilde{y}} U_B(y) \int_{\xi_0}^{\xi} (\xi - \tilde{\xi}) \mathrm{Ai}(\tilde{\xi}) \mathrm{d}\tilde{\xi} / y. \tag{4.29}$$

from (3.6) and (4.12). Note that we also have to use the upper-deck solution $v \sim \mathrm{e}^{\mathrm{i}m\tilde{y}}$ because the validity of the main-deck solution for v, unlike that for u, does not extend to the upper deck. Expressions (4.28) and (4.29) describe the modal shape of a T-S wave in the entire boundary layer.

For the stratification parameter $\hat{s} = 1.94$, the locally most unstable mode has the normalized frequency $\omega \approx 8.0$. However, this mode does not necessarily represent the locally most predominant disturbance observed, because for a spatial developing mode of fixed physical frequency to be dominant at an observation location, it must have already gained a large amplitude through substantial amplification upstream. Its normalized local frequency must be greater than 8.0 because of the thickening of the boundary layer. In our calculation, we choose $\omega = 30.0$. The wavelength of this mode is about 1.8 m, close to the wavelengths (approximately 1–2 m) of the observed disturbances in the experiment (Ohya & Uchida 2003). The distribution of the streamwise and normal velocities is shown in figure 5. Since linear stability theory cannot predict the absolute amplitude, $\widehat{v}_c$ and $\widehat{u}_c$ are normalized such that their maximum is unity. The predicted modal shape is characteristic of a wall mode, quite distinct from a K-H mode. The theoretical result clearly resembles the measurement. A better agreement is not warranted because of several complications. First, the disturbance in the experiment is uncontrolled and hence is most likely to be broadband in its nature, but the spectral content is unknown. Secondly, the wall shear extracted from the experimental data is not expected to be accurate, and indeed an error of 30 % cannot be ruled out. In view of these uncertainties, we also computed eigenfunctions using different values for ω (between 8 and 50) and λ (between 2 and 4), and found that the result is only moderately altered. Based on this level of agreement and the robustness of the modal shape, it seems reasonable to suggest that T-S instability operates in the experiment.

Before relating the theoretical findings to waves in the atmospheric boundary layer, we must address a difficult question: how might the assumption of a laminar base flow be justified? In nocturnal boundary layers, fluctuations are for most of the time quite weak, and turbulence is intermittent (Nakmura & Mahrt 2005). We believe that use of a laminar base flow is appropriate. In more general situations, waves and persistent small-scale turbulence coexist. Not only are the waves nonlinear, the Reynolds stresses contributed by these waves and turbulence act to alter the mean flow substantially. Yet, since these fully developed waves originate from the instability of a laminar state, a stability analysis of a laminar base flow might provide a qualitative estimate of their gross characteristics such as wavelength, frequency and propagation speed. Some investigators use instead a turbulent mean flow for stability calculations; however, this practice is not as straightforward as it looks. Because a turbulent profile is not a solution to the Navier–Stokes equations, the relevant stability equation (i.e. the Goldstein–Taylor, or Orr–Sommerfeld-like equation when viscosity is included) cannot be derived unless the effect of turbulence on instability waves is assumed to be negligible. Such an assumption has often been made implicitly without being acknowledged. In the case of inviscid instability, it may probably be justified as follows: suppose that an eddy-viscosity model is used to parameterize the small-scale effect, then the eddy viscosity, just like molecular viscosity, can be neglected since inviscid instability is sensitive to neither. For the present viscous instability, the logarithmic layer in the turbulent profile presents an additional complication. If the lower deck lies just underneath this layer, the assumed property (2.14) is not satisfied. In order for the analysis to be applicable, it must be further assumed that the lower deck is embedded well within a laminar sublayer. Whether a laminar or turbulent mean flow is used, the theory represents a drastic simplification of real atmospheric boundary layers, and so we can only expect it to capture some qualitative features of certain atmospheric waves.

Evidence of waves exhibiting the qualitative characteristics of the T-S instability may be found in some field observations. For example, waves with very large wavelengths (about 1–3 km) and long periods (5–10 min) have frequently been observed to reside in the first few tens to hundreds metres of the atmosphere, where the wind speed is in the range of 4 to $9\,\mathrm{m\,s^{-1}}$ (Caughey & Reading 1975; Eymard & Weill 1979; Einaudi *et al.* 1989). The propagation velocities of these waves are also somewhat small, between 0.3 and 0.5 of the maximum wind speed. They reside in the main bulk of the boundary layer (see figure 7*a* of Caughey & Reading 1975), and carry a strong momentum flux (Eymard & Weill 1979). These features are different from those of typical inviscid K-H modes, but are consistent with T-S waves. This is not surprising from the theoretical standpoint, because the long-wavelength nature implies that these waves are sensitive to the viscous effect exerted by the ground. It thus seems not unreasonable to suggest that these long waves arise owing to viscous instability. Unfortunately, the observational data in the literature are not detailed enough to enable us to make a firm connection.

5. Nonlinear stability and collapse of wave fronts

5.1. *Extended Benjamin–Davis–Ono equation*

In the high-frequency limit, $k \gg O(1)$, the spatial linear growth rate is vanishingly small (see (4.26)), and so is the temporal growth rate for $k > \hat{s}$ (see (4.23)). When such a nearly neutral instability mode amplifies, it will evolve through a series of weakly nonlinear stages, for which amplitude equations of the Landau–Stuart type

may be derived. However, similar to the non-stratified case ($\hat{s} = 0$) considered by Smith & Burggraf (1985), the coefficients of the nonlinear terms turn out to be purely imaginary with the consequence that the weakly nonlinear effect influences the phase but not the magnitude of the unstable mode. Following Smith & Burggraf (1985), we consider the strongly nonlinear stage.

Let $\partial/\partial T = O(\Omega) \gg O(1)$. Then the dispersion relation in the high-frequency limit, (4.21) or (4.25), implies that $\partial/\partial X = O(\Omega^{1/2}) \gg O(1)$. The above considerations suggest the introduction of the fast time and short space variables

$$\bar{T} = \Omega T, \quad \bar{X} = \Omega^{1/2} X. \tag{5.1}$$

In order to retain the stratification effect, the parameter $\hat{s}$ is rescaled as

$$\hat{s} = \Omega^{1/2}\bar{s} \quad \text{with} \quad \bar{s} = O(1).$$

The lower deck splits into two layers: an inviscid buffer layer with $Y \sim \Omega^{1/2}$ and a viscous sublayer where $Y \sim \Omega^{-1/2}$.

In the buffer layer, the appropriate transverse variable is $Z = \Omega^{-1/2}Y = O(1)$, and (U, V, P, A) expands as (Smith & Burggraf 1985)

$$(U, V, P, A) = \left(\Omega^{1/2}U^*, \Omega^{3/2}V^*, \Omega P^*, \Omega^{\frac{1}{2}}A^*\right) + \cdots. \tag{5.2}$$

Substitution of expansion (5.2) with (5.1) into (3.21)–(3.22) yields the inviscid equations

$$\frac{\partial U^*}{\partial \bar{X}} + \frac{\partial V^*}{\partial Z} = 0, \quad \frac{\partial U^*}{\partial \bar{T}} + U^*\frac{\partial U^*}{\partial \bar{X}} + V^*\frac{\partial U^*}{\partial Z} = -\frac{\partial P^*}{\partial \bar{X}}. \tag{5.3}$$

The matching condition (3.24) now reads

$$U^* \to \lambda(Z + A^*) \quad \text{as} \quad Z \to \infty \tag{5.4}$$

while the pressure–displacement relation becomes

$$P^*(\bar{X}, \bar{T}) = \int_{-\infty}^{\infty} \mathscr{G}(X;\xi)(\bar{s}|\bar{X} - \xi|)\left(A^*_{\xi\xi} + \bar{s}^2 A^*\right) \mathrm{d}\xi. \tag{5.5}$$

The functions

$$U^* = \lambda(Z + A^*), \quad V^* = -\lambda A^*_{\bar{X}} Z \tag{5.6}$$

satisfy both the continuity equation and matching condition (5.4). Substitution of these and (5.5) into the momentum equation in (5.3) yields a nonlinear equation for A^*,

$$\lambda\frac{\partial A^*}{\partial \bar{T}} + \lambda^2 A^*\frac{\partial A^*}{\partial \bar{X}} + \frac{\partial}{\partial \bar{X}}\int_{-\infty}^{\infty} \mathscr{G}(\bar{X};\xi)((A^*_{\xi\xi} + \bar{s}^2 A^*)\mathrm{d}\xi = 0. \tag{5.7}$$

The parameter λ can be eliminated by putting $A^* = \lambda^{-2}A^\dagger$ and $\bar{T} = \lambda T^\dagger$, so that (5.7) finally becomes

$$\frac{\partial A^\dagger}{\partial T^\dagger} + A^\dagger\frac{\partial A^\dagger}{\partial \bar{X}} + \frac{\partial}{\partial \bar{X}}\int_{-\infty}^{\infty} \mathscr{G}(X;\xi)(\bar{s}|\bar{X} - \xi|)(A^\dagger_{\xi\xi} + \bar{s}^2 A^\dagger)\mathrm{d}\xi = 0. \tag{5.8}$$

The viscous sublayer is described by the transverse variable $\bar{Z} = \Omega^{1/2}Y = O(1)$, and the solution expands as

$$(U, V, P, A) = \left(\Omega^{1/2}\bar{U}, \Omega^{1/2}\bar{V}, \Omega P^*, \Omega^{1/2}A^*\right) + \cdots. \tag{5.9}$$

Substitution of these with (5.1) into (3.21)–(3.22) shows that the full viscous nonlinear equations

$$\frac{\partial \bar{U}}{\partial \bar{X}} + \frac{\partial \bar{V}}{\partial \bar{Z}} = 0, \quad \frac{\partial \bar{U}}{\partial \bar{T}} + \bar{U}\frac{\partial \bar{U}}{\partial \bar{X}} + \bar{V}\frac{\partial \bar{U}}{\partial \bar{Z}} = -\frac{\partial P^*}{\partial \bar{X}} + \frac{\partial^2 \bar{U}}{\partial \bar{Z}^2}, \tag{5.10}$$

are reinstated. This is a system of classical boundary-layer equations because the pressure P^* is given by (5.5). Since viscous diffusion appears at leading order, the boundary conditions

$$\bar{U} = \bar{V} = 0 \quad \text{at} \quad \bar{Z} = 0, \tag{5.11}$$

can be imposed. Matching with the buffer layer requires that

$$\bar{U} \to \lambda A^* \quad \text{as} \quad \bar{Z} \to \infty. \tag{5.12}$$

It is worth noting that taking the limit $\bar{Z} \to \infty$ in the momentum equation (5.10) and using (5.12) and (5.5), also lead to evolution equation (5.7).

For $\bar{s} \ll 1$, the Bessel and Struve functions Y_0 and $\boldsymbol{H}_0$ in $\mathscr{G}$ may be approximated by their asymptotes for $\bar{s}\bar{X} \ll O(1)$, namely, $Y_0(\bar{s}\bar{X}) \sim (2/\pi)\ln(\bar{s}\bar{X})$ and $\boldsymbol{H}_0(\bar{s}\bar{X}) \sim \bar{s}\bar{X}/(2\pi)$, use of which in (5.8) reduces it to the original BDO equation (Smith & Burggraf 1985)

$$\frac{\partial A^\dagger}{\partial T^\dagger} + A^\dagger \frac{\partial A^\dagger}{\partial \bar{X}} + \frac{1}{\pi}\int_{-\infty}^{\infty} \frac{A^\dagger_{\xi\xi}}{\bar{X} - \xi} \mathrm{d}\xi = 0. \tag{5.13}$$

For this reason, (5.8) will be referred to as an extended BDO equation. This equation may arise in a variety of flows. For example, by generalizing the model of Benjamin (1967), Davis & Acrivos (1967) and Ono (1975) to include a weak density stratification in the layer of infinite depth, Maslowe & Redekopp (1980) and Romanova (1981) derived the evolution equation equivalent to (5.8) (with the present form being somewhat simpler than theirs). A two-dimensional extension was obtained by Voronovich, Shrira & Stepanyants (1998). It is, however, worth noting that in these studies the leading-order propagation speed is predicted by linear theory describing the waveguide property of the shear layer, and is generally comparable with the characteristic speed of the background flow. There the nonlinear effect merely provides a higher-order correction. The waves described by the present theory are of a different kind in that their propagation speeds are much smaller than the base flow, and are influenced by nonlinearity at leading order.

In the limit $\bar{s} = 0$, the BDO equation admits the well-known algebraic solitary solution

$$A^\dagger(\bar{X}, T^\dagger) = \frac{a}{1 + c^2(\bar{X} - cT^\dagger)^2}, \tag{5.14}$$

where the propagation speed c is related to the amplitude a via

$$c = a/4. \tag{5.15}$$

However, for $\bar{s} \neq 0$, following Maslowe & Redekopp (1980), it can be shown that

$$\frac{\partial}{\partial T^\dagger}\int_{-\infty}^{\infty} A^{\dagger 2} \mathrm{d}\bar{X} = -\int_0^{\bar{s}} k\sqrt{\bar{s}^2 - k^2}\, |a^\dagger(k, T^\dagger)|^2 \mathrm{d}k, \tag{5.16}$$

where $a^\dagger(k, T^\dagger)$ denotes the Fourier transform of $A^\dagger$, and in the derivation the integral representation (3.18) for $\mathscr{G}$ was used. The result (5.16) indicates that radiating components in the wavenumber band $-\bar{s} < k < \bar{s}$ appear as energy drain, and a (spatially compact) perturbation must decay owing to radiation of gravity waves

(Maslowe & Redekopp 1980; Romanova 1981). A solitary-wave solution thus no longer exists. On the other hand, it will be shown in Part 2 that an extended BDO equation with forcing may be derived, in which the incoming gravity waves in the outer flow may act as a driving term. If these waves propagate at a common speed, they may excite within the boundary-layer disturbances which may appear to be solitary.

5.2. *Numerical solutions*

Equation (5.8) as a potentially generic equation clearly warrants a thorough investigation. In the present paper, a preliminary study will be made. We solve (5.8) numerically using a spectral method, which is convenient and also aids the interpretation of numerical results. For the purpose of illustration, the initial condition is taken to be (5.14), and the stratification parameter $\bar{s} = 0.5$. Both the initial profile (5.14) and equation (5.8) are Fourier transformed with respect to $\bar{X}$, and the resulting equation for $a^{\dagger}(k, T^{\dagger})$ in the spectral space k is truncated for $k \in [-K, K]$. A fourth-order Runge–Kutta scheme is used to obtain $a^{\dagger}(k, T^{\dagger})$ at subsequent time $T^{\dagger}$, which is then inverted to find $A^{\dagger}(\bar{X}, T^{\dagger})$.

The spatial distribution of the disturbance at three different times is displayed in figure 6. As expected, the overall magnitude of the disturbance decays because of energy loss caused by radiation of gravity waves. Oscillations or ripples of relatively short scale soon appear on the front of the initially isolated disturbance. These oscillations propagate downstream, and become stronger as time increases. At $T^{\dagger} = 2$, the original peak is no longer dominant, and the front has almost collapsed completely, replaced by a quite well-developed wavepacket of shorter wavelength. In this sense, the front may be said to be locally unstable. A careful resolution check was carried out to ensure that the oscillations were well resolved. The results shown here were obtained with $K = 8$, the time step $\Delta T^{\dagger} = 10^{-3}$ and spectral discretization parameter $\Delta k = 10^{-2}$. The results do not change when $K = 8$ is increased to 16, or when either Δk or $\Delta \bar{X}$ is halved.

The reason that the oscillations arise becomes clear when we examine the evolution of spectrum $a^{\dagger}(k, T^{\dagger})$. As shown in figure 7, the energy of the radiating components in the wavenumber band $k \in (-s, s)$ decreases, but the (Fourier) spectral components with wavenumbers $|k| > s$ develop to acquire appreciable magnitudes. The appearance of the oscillations is associated with these components, because when the latter are filtered out in the Fourier inversion, ripples are found to disappear. The fact that the energy in the high-wavenumber components has almost diminished completely indicates that the spectral bandwidth is large enough to achieve convergence.

We also calculated the pressure field of the radiated gravity waves by inverting (3.15). Figure 8 shows the contours of the pressure field at $T^{\dagger} = 0$ and 1. The emitted gravity waves are highly directional; they form a beam, which is almost vertical. The gross character of the radiation remains almost intact at later times, despite the appearance of the ripples. This is not surprising, because those ripples are associated with non-radiating components.

6. Triple deck theory for jet-like profiles

The viscous instability described in § 4 is robust in the sense that the leading-order dispersion relation is controlled by the surface shear λ and is independent of the detailed distribution provided $u_{\infty} = O(1)$. However, for $u_{\infty} \ll O(1)$, the scaling and the instability property undergo significant changes. In the extreme case, $u_{\infty} = 0$, the

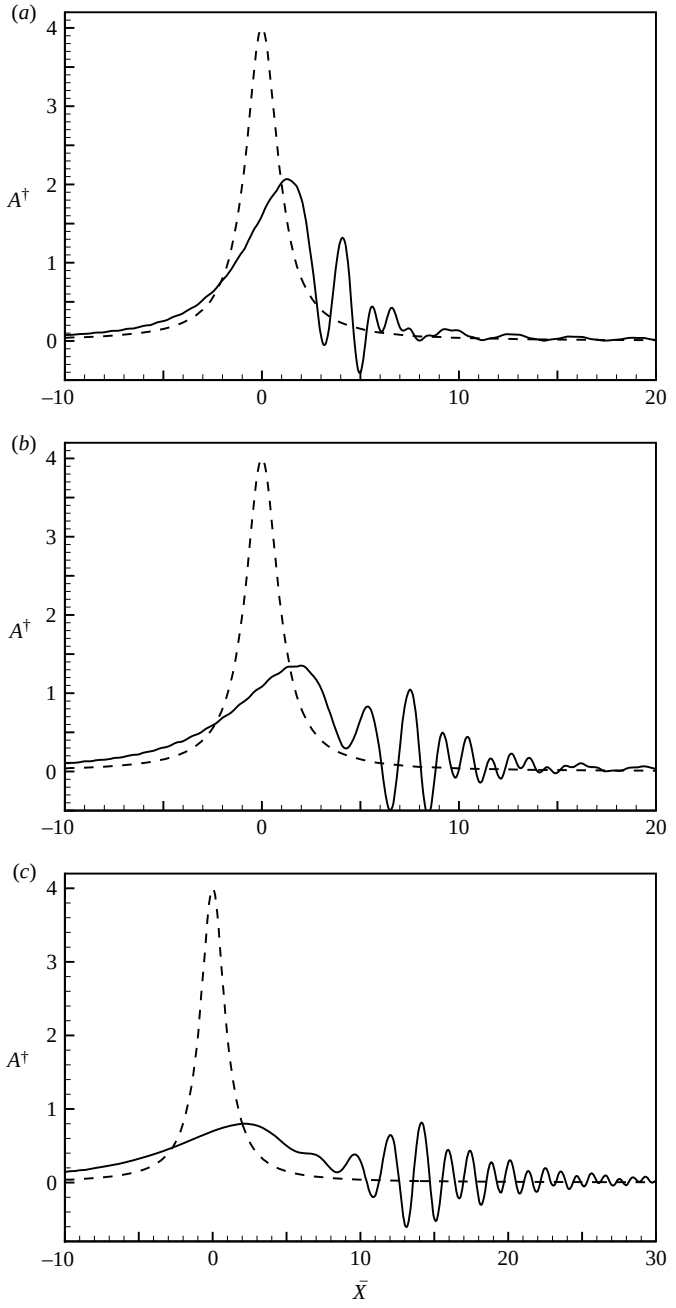

FIGURE 6. The profile of the disturbance: $A^\dagger(\bar{X}, T^\dagger)$ *vs.* $\bar{X}$ at (*a*) $T^\dagger = 0.5$, (*b*) 1.0 and (*c*) 2.0. The dashed lines represent the initial condition (5.14).

triple-deck structure is reduced to a double-deck one and the pressure–displacement relation becomes $P \sim A_{XX}$ instead of (3.17) (Smith & Duck 1977). Jet-like profiles with small $u_\infty \ll O(1)$ frequently arise in the atmospheric boundary layer (e.g. Mastrantonio *et al.* 1976). They possess inflection points and hence can support short-scale inviscid instability whose wavelength is comparable with the width of the shear layer. Our interest is in long-wavelength viscous instability. Specifically,

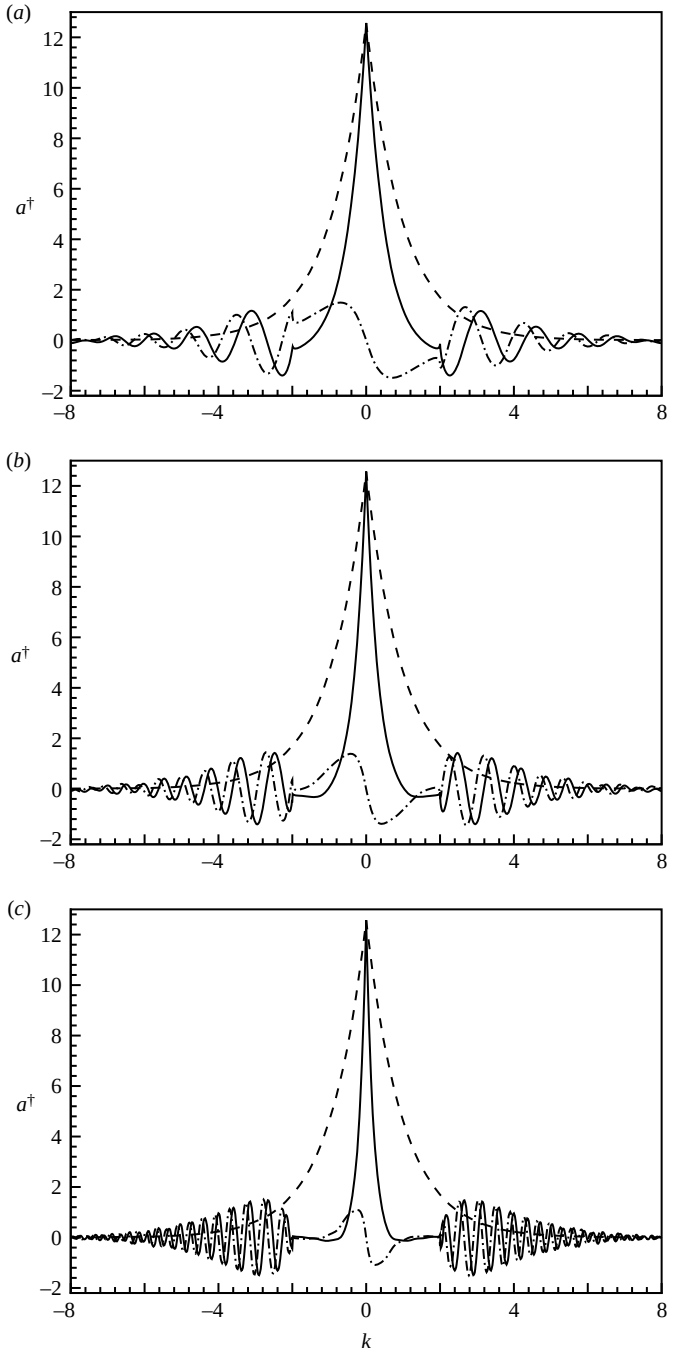

FIGURE 7. Evolution of the disturbance spectrum: $a^\dagger(k, T^\dagger)$ *vs.* k at (*a*) $T^\dagger = 0.5$, (*b*) 1.0 and (*c*) 2.0. Solid lines: real part $a_r^\dagger(k, T^\dagger)$; dashed-dotted lines: imaginary $a_i^\dagger(k, T^\dagger)$. The dashed lines represent spectrum of the initial condition (5.14).

we consider the distinguished regime which 'bridges' the cases of $u_\infty = O(1)$ and $u_\infty = 0$. This regime is attained when the pressure variation across the main deck is comparable with the pressure generated in the upper deck. This requirement fixes the

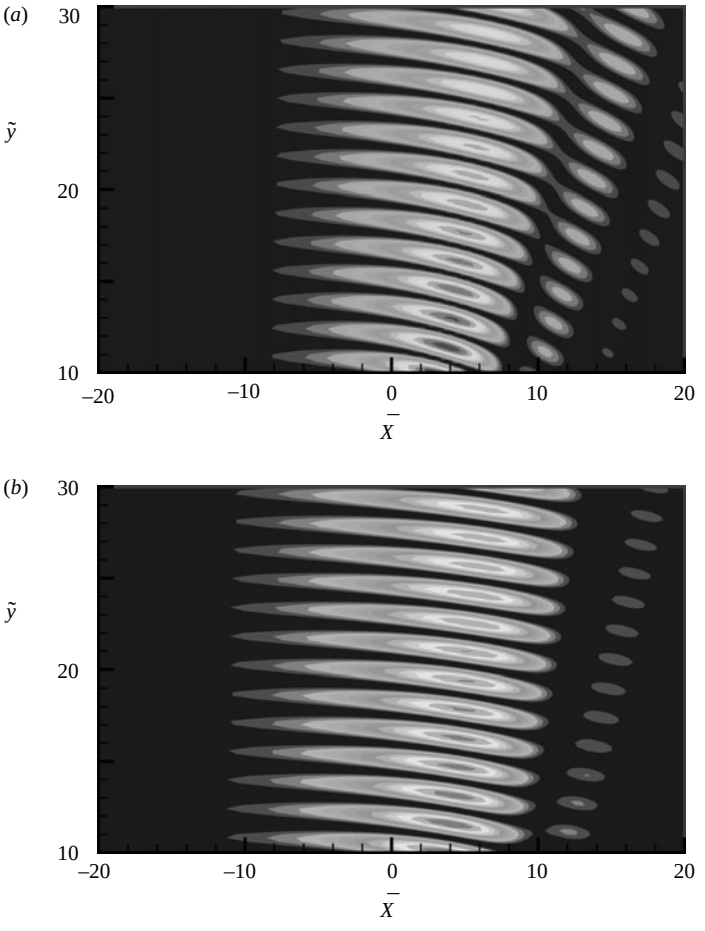

FIGURE 8. Radiation of gravity waves as shown by contours of the pressure field in the upper deck. (*a*) $T^{\dagger} = 0.5$; (*b*) $T^{\dagger} = 1.0$.

scaling for u_{∞} as

$$u_{\infty} = R^{-1/7}\chi \quad \text{with} \quad \chi = O(1). \tag{6.1}$$

The instability modes have characteristic wavelengths of $O(R^{1/7})$ and frequencies of $O(R^{-3/7})$, suggesting the introduction of the normalized space and time variables

$$X = \epsilon x, \quad T = \epsilon^3 t,$$

where throughout this section, the small parameter

$$\epsilon = R^{-1/7}. \tag{6.2}$$

The resulting modified triple-deck structure is shown in figure 1. The stratification parameter scales as

$$S = \epsilon^{3/2} s, \tag{6.3}$$

so that stratification effects appear in the upper deck only.

The disturbance in the main deck now expands as

$$(\tilde{u}, \tilde{v}, \tilde{p}, \tilde{\rho}) = \epsilon^2\{(U_1, \epsilon V_1, \epsilon^2 P_1, \rho_1) + \epsilon^2(U_2, \epsilon V_2, \epsilon^2 P_2, \rho_2) + \cdots\}. \tag{6.4}$$

The leading-order solution for the velocity and density remains the same as (3.6). One of the main differences from § 3 occurs in the pressure, which now satisfies

$$U_B \frac{\partial V_1}{\partial X} = -\frac{\partial P_1}{\partial y},$$

so that there is a normal pressure gradient across the main deck. P_1 has the solution

$$P_1 = P(X, T) + A_{XX} \int_0^y U_B^2 \mathrm{d}y, \tag{6.5}$$

with $P(X, T)$ being an arbitrary function. As $\tilde{y} \to \infty$,

$$P_1 \sim (P(X, T) - I A_{XX}) + \epsilon^2 \chi^2 y + \cdots, \tag{6.6}$$

where I is an $O(1)$ constant defined as

$$I = \int_0^\infty (u_\infty^2 - U_B^2) \mathrm{d}y.$$

For a jet-like profile, it turns out to be necessary to consider the second-order solution, U_2 and V_2, which satisfy

$$\frac{\partial U_2}{\partial X} + \frac{\partial V_2}{\partial y} = 0, \quad U_B \frac{\partial U_2}{\partial X} + U_B' V_2 = -A_T U_B' - \frac{\partial P_1}{\partial X}. \tag{6.7a,b}$$

After eliminating U_2, and solving the resultant equation for V_2, we find that

$$V_2 = -A_{2,X} U_B - A_T + U_B \Bigg\{ A_{XXX} \int_a^y \left(I + \int_0^y U_B^2 \mathrm{d}\hat{y} \right) \frac{\mathrm{d}y}{U_B^2} + (P_X - I A_{XXX}) \Big[\int_\infty^y \left(\frac{1}{U_B^2} - \frac{1}{\epsilon^2 \chi^2} \right) \mathrm{d}y + \frac{y}{\epsilon^2 \chi^2} \Big] \Bigg\}, \tag{6.8}$$

where A_2 is an $O(1)$ arbitrary function of X, and $a \neq 0$ an arbitrary constant. It follows that as $y \to \infty$, $V_2 \sim (P_X - I A_{XXX}) y / (\epsilon \chi) + O(1)$ and so

$$\tilde{v} \sim \epsilon^4 \chi (-A_X). \tag{6.9}$$

The solution for U_2 can be obtained from (6.7a), and it can be shown that for $y \ll 1$,

$$U_2 \sim \epsilon^{-2} (P - I A_{XX}) \lambda (J - y/\chi^2) + P U_B''(0) \lambda^{-2} \left(\ln y + \tfrac{3}{2} + O(y \ln y) \right) + \cdots,$$

where J denotes the Pearce integral

$$J = \int_0^\infty \left(\frac{\epsilon^2}{U_B^2} - \frac{1}{\chi^2} - \frac{\epsilon^2}{\lambda^2 y^2} \right) \mathrm{d}y.$$

This integral is regular if $U_B''(0) = 0$ (i.e. if the mean pressure gradient is zero), but is singular and hence must be interpreted as a Hadamard finite part if $U_B''(0) \neq 0$. Note that for a jet-like profile under consideration, the integrand is $O(1)$ so that J is $O(1)$ rather than $O(\epsilon^2)$. As a consequence, the slip velocity in $\epsilon^2 U_2$ is comparable with U_1, and

$$\tilde{u} \sim \epsilon^2 \lambda \{ A + J(P - I A_{XX}) \}.$$

The extra term represents the displacement induced by the inviscid flow in the main deck. This now becomes a leading-order effect as opposed to being a high-order correction in the usual case where $u_\infty = O(1)$.

In the upper deck, the transverse variable $\tilde{y} = \epsilon y = O(1)$, and the perturbation expands as

$$(\tilde{u}, \tilde{v}, \tilde{p}, \tilde{\rho}) = (\epsilon^4 \hat{U}, \epsilon^4 \hat{V}, \epsilon^4 \hat{P}, \epsilon^2 \hat{\rho}) + \cdots. \tag{6.10}$$

Substituting (2.15) along with (6.10) and (6.3) into (2.10)–(2.13) yields the same equations as (3.9)–(3.12) provided that u_∞ is replaced by χ. It follows that $\hat{P}$ satisfies the same equation as (3.13) except that

$$\hat{s} = s/\chi.$$

The boundary condition that $\partial \hat{P}/\partial \tilde{y} = \chi^2(A_{XX} + \hat{s}^2 A)$ remains intact in view of (6.9). Thus with the right correspondence of the parameters, the solution for $\hat{P}$ is identical to that given in § 3.3. Matching $\hat{P}$ with the main-deck solution (see (6.6)), we obtain the pressure–displacement relation

$$P(X, T) = I A_{XX} + \chi^2 \int_{-\infty}^{\infty} \mathscr{G}(X; \xi)(A_{\xi\xi}(\xi, T) + \hat{s}^2 A(\xi, T))\mathrm{d}\xi. \tag{6.11}$$

The first term on the right-hand side represents the pressure jump across the main deck, while the second term is the pressure induced in the upper deck.

The appropriate transverse coordinate in the lower deck is $Y = y/\epsilon^2$. The total flow field takes the form

$$(u, v, p, \rho) = (\epsilon^2 U, \epsilon^5 V, \epsilon^4 P, \epsilon^2 \rho) + \cdots. \tag{6.12}$$

The governing equations are (3.21)–(3.22), and the boundary condition (3.23) remains intact, but the matching requirement with the main deck now becomes (cf. (3.24))

$$U \to \lambda\Big\{Y + A + \chi^2 J \int_{-\infty}^{\infty} \mathscr{G}(X; \xi)\big(A_{\xi\xi} + \hat{s}^2 A\big)\mathrm{d}\xi\Big\} \quad \text{as} \quad Y \to \infty. \tag{6.13}$$

In addition to a different scaling, the present inviscid–viscous interaction for a jet-like flow differs from the standard one in that the main deck plays a more active role, namely, it contributes both a displacement effect and a normal pressure gradient. As a result, the pressure induced in the inviscid upper deck, rather than acting entirely on the viscous motion, is 'cushioned' by the pressure jump across the main deck. Conversely, the displacement generated by the viscous motion, is 'augmented' by the main-deck motion instead of being directly transmitted to the upper deck.

In the non-stratified case ($\hat{s} = 0$), the integral term in (6.11) and (6.13) reduces to the familiar Hilbert transform. It should be mentioned that as with the standard triple-deck theory, the present inviscid–viscous interaction for jet-like profiles can be of general value. For instance, in addition to describing viscous instability, it may describe separation of a jet-like flow encountering an abrupt perturbation.

By the same procedure as in § 5, the following equation can be derived in the high-frequency limit:

$$\left.\begin{aligned} \frac{\partial \tilde{A}}{\partial T^\dagger} + \tilde{A}\frac{\partial \tilde{A}}{\partial \bar{X}} + I\frac{\partial^3 A^\dagger}{\partial \bar{X}^3} + \chi^2 \frac{\partial}{\partial \bar{X}} \int_{-\infty}^{\infty} \mathscr{G}(X; \xi)\big(A^\dagger_{\xi\xi} + \hat{s}^2 A^\dagger\big)\mathrm{d}\xi = 0, \\ \tilde{A} = A^\dagger + \chi^2 J \int_{-\infty}^{\infty} \mathscr{G}(X; \xi)\big(A^\dagger_{\xi\xi} + \hat{s}^2 A^\dagger\big)\mathrm{d}\xi. \end{aligned}\right\} \tag{6.14}$$

If we set $J = 0$, then $\tilde{A} = A^\dagger$ and the equation is a combination of KdV and BDO equations in that it consists of both A_{XXX} and the integral term, which are

the dispersion terms appearing respectively in those two equations. Equation (6.14) may be referred to as a mixed KdV–BDO equation in the general case $J \neq 0$. Such equations do not appear to have been derived before, except that their special form with $J = 0$ was obtained by Romanova (1984).

7. Summary and concluding remarks

In this paper, we show that a stably stratified boundary layer can support viscous instability modes, which are a modified form of the well-known T-S waves. A triple-deck theory is presented to describe the linear and nonlinear evolutions of these modes. A linearized analysis was performed for both spatial and temporal instabilities. In the spatial formulation, stratification has a stabilizing effect in that it reduces the maximum growth rate. However, stratification does not stabilize all modes uniformly; there exists a band of modes whose growth rates are enhanced by stratification. In the temporal formulation, it is found, rather unexpectedly, that stratification actually increases the maximum growth rate. Both formulations show that increased stratification shifts the band of unstable modes towards high frequencies.

The nonlinear development of high-frequency/short-wavelength disturbances is studied. An extended BDO equation is derived from the fully nonlinear triple-deck system. As was shown in a related context (Maslowe & Redekopp 1980; Romanova 1981), where the same equation was derived, a spatially compact disturbance would decay because of the energy loss caused by radiation of long gravity waves. Our numerical solutions further suggest that when such an isolated disturbance decays, small-scale ripples develop on its front. An inward energy flux is thus required to compensate the energy loss if waves of permanent form are to be excited. Such a flux may be provided by incoming gravity waves.

A triple-deck theory is also presented for a jet-like profile with a vanishingly small free-stream velocity. It is shown that the inviscid–viscous interaction must include the displacement induced by the inviscid motion in the main deck as well as the pressure variation across the boundary layer. The nonlinear evolution of high-frequency disturbances is then governed by a mixed KdV–BDO equation.

T-S instability plays a fundamental role in laminar–turbulent transition of aerodynamic flows (such as the boundary layer around an airfoil), but its possible relevance in the atmospheric boundary layer remains unexploited. The present paper shows that the T-S mechanism continues to operate in the presence of stable stratification. It should therefore form part of the theoretical framework for understanding and interpreting wave activities in the atmosphere. On the basis of the theoretical results and available observational/experimental data, it was suggested that certain long-wavelength atmospheric disturbances, whose characteristics are not predicted well by inviscid instabilities, may instead be attributed to this viscous instability. Further laboratory and field investigations are required in order to establish conclusively the viscous origin of these waves. For that task, the present work may offer some useful guidance. For instance, the theory indicates that the principal parameter controlling T-S instability is the surface shear λ, (see the scaling relation (4.27)), and so it may be possible to identify the nature of the waves by studying the correlation between the characteristic frequency of the instability and λ.

The potential importance of the viscous instability will be further highlighted by the fact that it is coupled to gravity waves through topography, as will be shown in Part 2.

The authors would like to thank the referees for numerous helpful suggestions and for pointing out some key references. Most importantly, their careful scrutiny has helped the authors correct a significant error in the original manuscript.

This research was supported by the Natural Science Foundation of China (grant NSFC/10428206).

REFERENCES

Abramowitz, M. & Stegun, I. A. 1964 *Handbook of Mathematical Functions*. National Bureau of Standards.

Benjamin, T. B. 1967 Internal waves of permanent form in fluids of great depth. *J. Fluid Mech.* **29**, 559–592.

Benney, D. J. 1966 Long nonlinear waves in fluid flows. *J. Math. Phys.* **45**, 52–63.

Caughey, S. J. & Reading, C. J. 1975 An observation of waves and turbulence in the earth's boundary layer. *Boundary-Layer Met.* **9**, 279–296.

Chanin, M.-L. & Hauchecorne, A. 1981 Lidar observation of gravity and tidal waves in the stratosphere and mesosphere. *J. Geophys. Res.* **86**, 9715–9721.

Chimonas, G. 1970 The extension of the Miles–Howard theorem to compressible fluids. *J. Fluid Mech.* **43**, 833–836.

Chimonas, G. 1974 Consideration of the stability of certain heterogenrous shear flows incldluing some inflexion-free profiles. *J. Fluid Mech.* **65**, 65–69.

Chimonas, G. 1993 Surface drag instabilities in the atmospheric boundary layer. *J. Atmos. Sci.* **50**, 1914–1924.

Chimonas, G. 1995 Long-wavelength gravity instabilities: a comparison of the Geffrey's drag mechanism with the shear instability. *J. Atmos. Sci.* **52**, 191–195.

Chimonas, G. 2002 On internal gravity waves associated with the stable boundary layer. *Boundary-Layer Met.* **102**, 139–155.

Chimonas, G. & Grant, J. R. 1984 Shear excitation of gravity waves. Part I: Modes of a two-scale atmosphere. *J. Atmos. Sci.* **41**, 2269–2277.

Christie, D. R. 1989 Long nonlinear waves in the lower atmosphere. *J. Atmos. Sci.* **46**, 1462–1491.

Coulter, R. L. & Doran, J. C. 2002 Spatial and temporal occurrence of intermittent turbulence during CASES-99. *Boundary-Layer Met.* **105**, 329–349.

Davis, R. E. & Acrivos, A. 1967 Solitary internal waves in deep water. *J. Fluid Mech.* **29**, 593–607.

Davis, P. A. & Peltier, W. R. 1976 Resonant parallel shear instability in the stratified planetary boundary layer. *J. Atmos. Sci.* **33**, 1287–1300.

Davis, P. A. & Peltier, W. R. 1977 Effects of dissipation on parallel shear instability near the ground. *J. Atmos. Sci.* **34**, 1868–1884.

Davis, P. A. & Peltier, W. R. 1979 Some characteristics of the Kelvin–Helmholtz and resonant overreflection modes of shear flow instability and of their interaction through vortex pairing. *J. Atmos. Sci.* **36**, 2394–2412.

Drazin, P. G. & Howard, L. N. 1966 Hydrodynamic stability of parallel flow of inviscid fluids. *Adv. Appl. Mech.* **9**, 1–89.

Drazin, P. G. & Reid, W. H. 1981 *Hydrodynamic Stability*. Cambridge University Press.

Einaudi, F., Bedard, Jr, A. J. & Finnigan, J. J. 1989 A climatology of gravity waves and other coherent disturbances at the Boulder atmospheric observatory during March–April 1984. *J. Atmos. Sci.* **46**, 303–329.

Eymard, L. & Weill, A. 1979 A study of gravity waves in the planetary boundary layer by acoustic sounding. *Boundary-Layer Met.* **17**, 231–245.

Fabrikant, A. L. & Stepanyants, Yu. A. 1998 Propagation of waves in shear flows. World Scientific.

Gear, J. A. & Grimshaw, R. 1983 A second-order theory for solitary waves in shallow fluids. *Phys. Fluids* **26**, 14–29.

Goldstein, S. 1931 On the stability of superposed streams of fluid of different densities. *Proc. R. Soc. Lond.* A **132**, 524–548.

Gossard, E. E. & Hooke, W. H. 1975 *Waves in the Atmosphere*. Elsevier.

Grimshaw, R. 1981 A second-order theory for solitary waves in deep fluids. *Phys. Fluids* **24**, 1611–1618.

Howard, L. N. 1961 Note on a paper of John Miles. *J. Fluid Mech.* **10**, 509–512.

Lalas, D. P. & Einaudi, F. 1976 On the characteristics of gravity waves generated by atmospheric shear layer. *J. Atmos. Sci.* **33**, 1248–1259.

Lalas, D. P., Einaudi, F. & Fua, D. 1976 The destabilizing effect of the ground on Kelvin–Helmholtz waves in the atmosphere. *J. Atmos. Sci.* **33**, 59–69.

Lighthill, D. 1978 *Waves in Fluids*. Cambridge University Press.

Lilly, D. K. & Zipser, E. J. 1972 The front range windstorm of 11 January 1972. A meteorological narrative. *Weatherwise* **25**, 56–63.

Lindzen, R. S. 1981 Turbulence and stress owing to gravity wave and tidal breakdown. *J. Geophys. Res.* **86**, 9707–9714.

Maslowe, S. A. & Redekopp, L. G. 1980 Long nonlinear waves in stratifiled shear flows. *J. Fluid Mech.* **101**, 321–348.

Mastrantonio, G., Einaudi, F., Fua, D. & Lalas, D. P. 1976 Generation of gravity waves by jet streams in the atmosphere. *J. Atmos. Sci.* **33**, 1730–1738.

Merrill, J. T. 1977 Observational and theoretical study of shear instability in the airflow near the ground. *J. Atmos. Sci.* **34**, 911–921.

Miles, J. W. 1961 On the stability of heterogeneous shear flows. *J. Fluid Mech.* **10**, 496–508.

Mureithi, E. W. 1997 Effects of thermal bouyancy on the stability properties of boundary-layer flows. PhD thesis, University of New South Wales, Austrialia.

Mureithi, E. W., Denier, J. P. & Stott, J. A. K. 1997 The effect of buoyancy on upper branch Tollmien–Schlichting waves. *IMA J. Appl. Maths* **58**, 19–50.

Nakmura, R. & Mahrt, L. 2005 A study of intermittent turbulence with CASES-99 tower measurements. *Boundary-Layer Met.* **114**, 367–387.

Newsom, R. K. & Banta, R. W. 2003 Shear-flow instability in the stable boundary layer as observed by Doppler lidar during CASES-99. *J. Atmos. Sci.* **60**, 16–33.

Ohya, Y. & Uchida, T. 2003 Turbulence structure of stable boundary layers with a linear temperature profile. *Boundary-Layer Met.* **108**, 19–38.

Ono, H. 1975 Algebraic solitary waves in stratified fluids. *J. Phys. Soc. Japan* **39**, 1082–1091.

Queney, P. 1948 The problem of air flow over mountains: a summary of theoretical studies. *Bull. Am. Met. Soc.* **29**, 16–26.

Ralph, F. M., Neiman, P. J. & Levinson, D. 1997 Lidar observations of a breaking mountain wave associated with extreme turbulence. *Geophys. Res. Lett.* **24**, 663–666.

Romanova, N. N. 1981 Generalization of the Benjamin–Ono equation for a weakly stratified atmosphere. *Izv. Atmos. Ocean. Phys.* **17**, 98–101.

Romanova, N. N. 1984 Long nonlinear waves on layers having large wind velocity gradient. *Izv. Atmos. Ocean. Phys.* **20**, 452–456.

Rottman, J. W. & Einaudi, F. 1993 Solitary waves in the atmosphere. *J. Atmos. Sci.* **50**, 2116–2136.

Rottman, J. W. & Grimshaw, R. 2002 *Environmental Stratified Flows*. Kluwer.

Scorer, R. S. 1949 Theory of waves in the lee of mountains. *Q. J. R. Met. Soc.* **75**, 41–56.

Smith, F. T. 1973 Laminar flow over a small hump on a flat plate. *J. Fluid Mech.* **57**, 803–824.

Smith, F. T. 1979 On the non-parallel flow stability of the Blasius boundary layer. *Proc. R. Soc. Lond.* A **336**, 91–109.

Smith, F. T. & Burggraf, O. R. 1985 On the development of large-sized short-scaled disturbances in boundary layers. *Proc. R. Soc. Lond.* A **399**, 25–55.

Smith, F. T. & Duck, P. W. 1977 Separation of jets or thermal boundary layers from a wall. *Q. J. Mech. Appl. Maths* **30**, 145–156.

Smith, R. B., Skubis, S., Doyle, J. D., Broad, A. S., Kiemle, C. & Volkert, H. 2002 Mountain waves over Mont Blanc: influence of a stagnant boundary layer. *J. Atmos. Sci.* **59**, 2073–2092.

Smith, R. K. 1988 Travelling waves and bores in the lower atmosphere: the 'morning glory' and the related phenomenon. *Earth-Sci. Rev.* **25**, 267–290.

Smith, S. A. 2003 Observations and simulations of the 8 November MAP mountain wave case. *Q. J. R. Met. Soc.* **128**, 1–21.

Stewartson, K. 1974 Multistructured boundary layers on flat plates and related bodies. *Adv. Appl. Mech.* **14**, 145–239.

Stull, R. B. 1988 *An Introduction to Boundary Layer Meteorology*. Kluwer.

Sun, J., Burns, S. P., Lenschow, D. H., Banta, R., Newsom, R., Coulter, R., Frasier, S., Ince, T., Nappo, C., Cuxart, J., Blumen, W., Lee, X. & Hu, X. 2002 Intermittent turbulence associated with a density current passage in the stable boundary layer. *Boundary-Layer Met*. **105**, 199–219.

Sun, J., Lenschow, D. H., Burns, S. P., Newsom, R., Coulter, R., Frasier, S., Ince, T., Nappo, C., Balsley, R. B., Jensen, M., Mahrt, L., Miller, D. & Skelly, B. 2004 Atmospheric disturbances that generate intermittent turbulence in nocturnal boundary layers. *Boundary-Layer Met*. **110**, 255–279.

Sykes, R. I. 1978 Stratified effects in boundary layer flow over hills. *Proc. R. Soc. Lond*. A **361**, 225–243.

Sykes, R. I. 1980 On three-dimensional boundary layer flow over surface irregularities. *Proc. R. Soc. Lond*. A **373**, 311–329.

Taylor, G. I. 1931 Effect of variation in density on the stability of superposed streams of fluids. *Proc. R. Soc. Lond*. A **132**, 499–523.

Thorpe, S. A. 1969 Neutral eigensolutions of the stability equation for stratified shear flow. *J. Fluid Mech*. **36**, 673–683.

Voronovich, V. V., Shrira, V. I. & Stepanyants, Yu. A. 1998 Two-dimensional models for nonlinear vorticity waves in shear flows. *Stud. Appl. Maths* **100**, 1–32.

Wood, N. 2000 Wind flow over complex terrain: a historical perspective and the prospect for large-eddy modelling. *Boundary-Layer Met*. **96**, 11–32.

Wu, X. & Zhang, J. 2008 Instability of a stratified boundary layer and its coupling with internal gravity waves. Part 2. Coupling with internal gravity wavesvia topography. *J. Fluid Mech*. **595**, 409–433.

Wurtele, M. G. 1970 Meteorological conditions surrounding the paradise crash of 1 March 1964. *J. Appl. Met*. **9**, 787–795.